Ratios of $W^{\pm}\gamma$ and $Z\gamma$ cross sections: New tools in probing the weak boson sector at the Fermilab Tevatron

U. Baur
Physics Department, Florida State University, Tallahassee, Florida 32306

S. Errede
Physics Department, University of Illinois, Urbana, Illinois 61801

J. Ohnemus
Physics Department, University of Durham, DH1 3LE, England

(Received 12 April 1993)

The ratios $\mathcal{R}_{\gamma,l}=B(Z\to l^+l^-)\sigma(Z\gamma)/B(W\to l\nu)\sigma(W^{\pm}\gamma)$, $\mathcal{R}_{\gamma,\nu}=B(Z\to\bar{\nu}\nu)\sigma(Z\gamma)/B(W\to l\nu)\sigma(W^{\pm}\gamma)$, $\mathcal{R}_{W\gamma}=\sigma(W^{\pm}\gamma)/\sigma(W^{\pm})$, and $\mathcal{R}_{Z\gamma}=\sigma(Z\gamma)/\sigma(Z)$ are studied as tools to probe the electroweak boson self-interactions. As a function of the minimum photon transverse momentum, $\mathcal{R}_{\gamma,l}$ and $\mathcal{R}_{\gamma,\nu}$ are found to directly reflect the radiation zero present in $W^{\pm}\gamma$ production in the standard model. All four ratios are sensitive to anomalous $WW\gamma$ and/or $ZZ\gamma/Z\gamma\gamma$ couplings. The sensitivity of the cross-section ratios to the cuts imposed on the final-state particles, as well as the systematic uncertainties resulting from different parametrizations of parton distribution functions, the choice of the factorization scale Q^2, and from higher-order QCD corrections, are explored. Taking into account these uncertainties, sensitivity limits for anomalous three gauge boson couplings, based on a measurement of the cross-section ratios with an integrated luminosity of 25 pb^{-1} at the Fermilab Tevatron, are estimated.

PACS number(s): 13.85.Qk, 12.38.Bx, 13.38.+c, 14.80.Er

I. INTRODUCTION

The present run of the Fermilab Tevatron $p\bar{p}$ collider is expected to result in a substantial increase of the integrated luminosity. The increase in statistics will make it possible to observe new reactions such as $W^{\pm}\gamma$ and $Z\gamma$ production, and to probe previously untested sectors of the standard model (SM) of electroweak interactions, in particular, the vector boson self-interactions. Within the SM, at the tree level, these self-interactions are completely fixed by the SU(2)×U(1) gauge theory structure of the model. Their observation is thus a crucial test of the model. In contrast with low-energy and high-precision experiments at the Z peak, collider experiments offer the possibility of a direct, and essentially model-independent, measurement of the three vector boson vertices. For a detailed investigation at the Fermilab Tevatron, based on differential cross-section distributions, an integrated luminosity of at least 100 pb^{-1} is required [1,2]. For smaller data samples the total cross section is also useful.

In hadron collider experiments, cross-section measurements are usually plagued by large experimental systematic and theoretical errors. These errors, however, can often be significantly reduced by considering ratios of cross sections. A well-known example is the ratio

$$\mathcal{R}_l=\frac{\sigma(W^{\pm}\to l^{\pm}\nu)}{\sigma(Z\to l^+l^-)}=\frac{B(W\to l\nu)\sigma(W^{\pm})}{B(Z\to l^+l^-)\sigma(Z)} \tag{1.1}$$

of the observable $W^{\pm}$ and Z cross sections [3]. Here, $l=e,\mu$, $B(W\to l\nu)$, and $B(Z\to l^+l^-)$ denote the leptonic branching ratios of the W and Z bosons, respectively, and $\sigma(W^{\pm})$ [$\sigma(Z)$] is the $W^{\pm}$ (Z) production cross section in $p\bar{p}$ collisions. The systematic error of $\mathcal{R}_l$ is less than half that of the individual cross sections $B(W\to l\nu)\sigma(W^{\pm})$ and $B(Z\to l^+l^-)\sigma(Z)$ [4]. Using the SM expectation for the cross-section ratio $\sigma(W^{\pm})/\sigma(Z)$ together with information on the leptonic branching ratio of the Z boson from the CERN e^+e^- collider LEP, $B(W\to l\nu)$ can be determined from $\mathcal{R}_l$; in turn, this value of $B(W\to l\nu)$ can be translated into a model-independent lower limit on the top quark mass of $m_t>55$ GeV (95% C.L.) [4].

It is natural to consider cross-section ratios similar to that of Eq. (1.1) for $W^{\pm}\gamma$ and $Z\gamma$ production, and to use them to extract information on $WW\gamma$, $ZZ\gamma$, and $Z\gamma\gamma$ couplings. Four different ratios can be formed:

$$\mathcal{R}_{\gamma,l}=\frac{B(Z\to l^+l^-)\sigma(Z\gamma)}{B(W\to l\nu)\sigma(W^{\pm}\gamma)}\ , \tag{1.2}$$

$$\mathcal{R}_{\gamma,\nu}=\frac{B(Z\to\bar{\nu}\nu)\sigma(Z\gamma)}{B(W\to l\nu)\sigma(W^{\pm}\gamma)}\ , \tag{1.3}$$

$$\mathcal{R}_{W\gamma}=\frac{B(W\to l\nu)\sigma(W^{\pm}\gamma)}{B(W\to l\nu)\sigma(W^{\pm})}=\frac{\sigma(W^{\pm}\gamma)}{\sigma(W^{\pm})}\ , \tag{1.4}$$

and

$$\mathcal{R}_{Z\gamma}=\frac{B(Z\to l^+l^-)\sigma(Z\gamma)}{B(Z\to l^+l^-)\sigma(Z)}=\frac{\sigma(Z\gamma)}{\sigma(Z)}\ . \tag{1.5}$$

Similar ratios have also been proposed for $W^{\pm}+n$ jet and $Z+n$ jet, $n=1,\ldots,3$, production [5]. The $W^{\pm}\gamma$ and $Z\gamma$ cross-section ratios are related to $\mathcal{R}_l$ of Eq. (1.1)

through the relation

$$\mathcal{R}_l \mathcal{R}_{\gamma,l} = \frac{\mathcal{R}_{Z\gamma}}{\mathcal{R}_{W\gamma}} \ . \tag{1.6}$$

Experimentally, the ratios of Eqs. (1.2)–(1.5) can be determined from independent data samples. $\mathcal{R}_{\gamma,l}$ can be measured from an event sample with at least one isolated, high transverse momentum electron (muon) and one isolated high p_T photon. $\mathcal{R}_{\gamma,\nu}$ can be determined from a data sample extracted with a missing transverse energy trigger and an additional isolated hard photon. Finally, $\mathcal{R}_{W\gamma}$ and $\mathcal{R}_{Z\gamma}$ can be obtained from the inclusive sample of W and Z boson candidates, respectively.

Many experimental uncertainties, for example, those associated with lepton and photon detection efficiencies, or the uncertainty in the integrated luminosity, are expected to cancel, at least partially, in the cross-section ratios. $\mathcal{R}_{W\gamma}$ and $\mathcal{R}_{Z\gamma}$ are independent of the vector boson branching ratios, and thus represent directly the ratio of $W^{\pm}\gamma$ to $W^{\pm}$ and $Z\gamma$ to Z cross sections. Since the cross section for W/Z production is much larger than the rate for $W\gamma/Z\gamma$ production, the statistical error of $\mathcal{R}_{W\gamma}$ and $\mathcal{R}_{Z\gamma}$ is expected to be significantly smaller than that of $\mathcal{R}_{\gamma,l}$ and $\mathcal{R}_{\gamma,\nu}$.

In this paper we study the theoretical aspects of the cross-section ratios shown in Eqs. (1.2)–(1.5). Our calculations are based on results presented in Refs. [1,2,6,8]. Cross sections in the Born approximation are obtained by calculating helicity amplitudes for the complete processes $q\bar{q}' \to W^{\pm}\gamma \to l^{\pm}\nu\gamma$, $q\bar{q} \to Z\gamma \to l^+l^-\gamma$, and $q\bar{q} \to Z\gamma \to \nu\bar{\nu}\gamma$, including the effects of timelike photon exchange diagrams and bremsstrahlung from the final-state lepton line. Finite W/Z width effects, and correlations between the final-state leptons originating from W/Z decay, are also fully incorporated in our calculations. In contrast, next-to-leading log QCD corrections to $W\gamma$ and $Z\gamma$ production are at present only known in the limit of stable, on-shell weak bosons [7,8].

In Sec. II, we consider the cross-section ratios (1.2)–(1.5) within the framework of the SM at Fermilab Tevatron energies. Experimentally, one measures the ratios

$$\tilde{\mathcal{R}}_{\gamma,l} = \frac{\sigma(l^+l^-\gamma)}{\sigma(l^{\pm}\nu\gamma)} \ , \tag{1.7a}$$

$$\tilde{\mathcal{R}}_{\gamma,\nu} = \frac{\sigma(\bar{\nu}\nu\gamma)}{\sigma(l^{\pm}\nu\gamma)} \ , \tag{1.7b}$$

$$\tilde{\mathcal{R}}_{W\gamma} = \frac{\sigma(l^{\pm}\nu\gamma)}{\sigma(l^{\pm}\nu)} \ , \tag{1.7c}$$

and

$$\tilde{\mathcal{R}}_{Z\gamma} = \frac{\sigma(l^+l^-\gamma)}{\sigma(l^+l^-)} \ , \tag{1.7d}$$

rather than $\mathcal{R}_{\gamma,l}$, $\mathcal{R}_{\gamma,\nu}$, and $\mathcal{R}_{V\gamma}$ ($V=W,Z$) directly. In order to isolate the cross-section ratios of Eqs. (1.2)–(1.5), appropriate cuts have to be imposed in order to suppress the contributions of final-state bremsstrahlung (radiative W/Z decays) to the $l\nu\gamma$ and $ll\gamma$ final states. These cuts are described in Sec. II A, together with other details of our calculation.

In Sec. II B, the ratios are studied as a function of the minimum photon transverse momentum $p_T^{\min}(\gamma)$ and the minimum $V\gamma$ ($V=W,Z$) invariant mass $m_{\min}$. As a function of $p_T^{\min}(\gamma)$, $\mathcal{R}_{\gamma,l}$ and $\mathcal{R}_{\gamma,\nu}$ are shown to directly reflect the radiation zero which is present in $W\gamma$ production in the SM [9]. In Sec. II B, we also investigate how the ratios depend on the cuts imposed on the final-state particles. The systematic and theoretical uncertainties of the cross-section ratios originating from the parametrization of the parton distribution functions, the choice of the factorization scale Q^2, and higher-order QCD corrections are studied in Sec. II C. The size of the QCD corrections can be reduced significantly by imposing a central jet veto cut. The theoretical and systematic uncertainties to the cross-section ratios are found to be well under control. $\mathcal{R}_{\gamma,l}$ and $\mathcal{R}_{\gamma,\nu}$ are significantly less sensitive to these uncertainties than $\mathcal{R}_{W\gamma}$ and $\mathcal{R}_{Z\gamma}$. The $W^{\pm}\gamma$ and $Z\gamma$ cross-section ratios thus possess the same advantages which make the ratio of W to Z boson cross sections, Eq. (1.1), a powerful tool for probing new physics, e.g., the extraction of a model-independent limit on the top quark mass [3,4].

In Sec. III, we study how nonstandard three gauge boson couplings affect the cross-section ratios. We also estimate the sensitivity limits for anomalous three vector boson couplings which one can hope to achieve from data accumulated in the current Fermilab Tevatron run, taking into account the systematic uncertainties to the ratios. Section IV, finally, contains our conclusions.

II. STANDARD MODEL $W^{\pm}\gamma$ AND $Z\gamma$ CROSS-SECTION RATIOS

A. Preliminaries

The signal in $p\bar{p} \to W^{\pm}\gamma/Z\gamma$ consists of an isolated high transverse momentum (p_T) photon and a $W^{\pm}$ or Z boson which may decay either hadronically or leptonically. The hadronic W and Z decays will be difficult to observe due to the QCD two jet $+\gamma$ background [10]. In the following we therefore focus on the leptonic decay modes of the weak bosons. The signal for $W^{\pm}\gamma$ production is then

$$p\bar{p} \to l^{\pm}\not{p}_T\gamma \ , \tag{2.1}$$

where $l=e,\mu$ (we neglect the τ decay mode of the W/Z) and the missing transverse momentum $\not{p}_T$ results from the nonobservation of the neutrino from the W decay. The signal for $Z\gamma$ production is

$$p\bar{p} \to l^+l^-\gamma \tag{2.2}$$

if the Z boson decays into a pair of charged leptons, and

$$p\bar{p} \to \not{p}_T\gamma \tag{2.3}$$

if the Z boson decays into a pair of neutrinos. In addition to the standard Feynman diagrams for $q\bar{q}' \to W\gamma$ and $q\bar{q} \to Z\gamma$, final-state bremsstrahlung diagrams contribute to (2.1) and (2.2). We incorporate their effects, to-

gether with those from timelike photon exchange diagrams contributing to (2.2), and finite W/Z width effects, in our numerical simulations of the lowest-order cross sections. All cross sections and dynamical distributions are evaluated using parton level Monte Carlo programs.

In order to simulate the finite acceptance of detectors we impose, unless stated otherwise, the following set of transverse momentum, pseudorapidity (η), and separation cuts:

$$p_T(\gamma) > 10 \text{ GeV}, \quad |\eta(\gamma)| < 3 ,$$
$$p_T(l) > 15 \text{ GeV}, \quad |\eta(l)| < 3.5 , \tag{2.4}$$
$$\not{p}_T > 15 \text{ GeV}, \quad \Delta R(l\gamma) > 0.7 .$$

Here,

$$\Delta R(l\gamma) = [(\Delta\Phi_{l\gamma})^2 + (\Delta\eta_{l\gamma})^2]^{1/2} \tag{2.5}$$

is the charged lepton photon separation in the pseudorapidity azimuthal angle plane. The cuts listed in Eq. (2.4) approximate the phase-space region covered by the Collider Detector at Fermilab (CDF) and D0 detectors at the Tevatron [11,12].

Because of the large separation cut, contributions from the final-state bremsstrahlung (radiative W/Z decay) diagrams to (2.1) and (2.2) are strongly suppressed. They can be eliminated almost completely by imposing the following additional cuts on the invariant mass of the lepton pair and the $ll\gamma$ system:

$$m_{ll} > 50 \text{ GeV}, \quad m_{ll\gamma} > 100 \text{ GeV} \tag{2.6}$$

in reaction (2.2) (Ref. [2]) and

$$m_{T(}l\gamma;\not{p}_T) > 90 \text{ GeV} \tag{2.7}$$

in reaction (2.1) (Ref. [1]) where

$$m_T^2(l\gamma;\not{p}_T) = \{[m_{l\gamma}^2 + |\mathbf{p}_T(\gamma) + \mathbf{p}_T(l)|^2]^{1/2} + \not{p}_T\}^2 - |\mathbf{p}_T(\gamma) + \mathbf{p}_T(l) + \not{\mathbf{p}}_T|^2 \tag{2.8}$$

is the square of the cluster transverse mass. In Eq. (2.8), $m_{l\gamma}$ denotes the invariant mass of the $l\gamma$ pair. The cuts listed in Eqs. (2.6) and (2.7) ensure that the experimentally measured cross-section ratios of Eq. (1.7) virtually coincide with the ratios listed in Eqs. (1.2)–(1.5). Therefore, we shall not discriminate between the two sets of ratios subsequently.

Uncertainties in the energy measurements of the charged leptons and the photon are taken into account in our numerical simulations by Gaussian smearing of the particle momenta with

$$\frac{\sigma}{E} = \begin{cases} 0.135/\sqrt{E_T} \otimes 0.02 & \text{for } |\eta| < 1.1, \\ 0.28/\sqrt{E} \otimes 0.02 & \text{for } 1.1 < |\eta| < 2.4, \\ 0.25/\sqrt{E} \otimes 0.02 & \text{for } 2.4 < |\eta| < 4.2 , \end{cases} \tag{2.9}$$

corresponding to the CDF detector resolution [11]. In Eq. (2.9), E (E_T) is the energy (transverse energy) of the particle and the symbol $\otimes$ signifies that the constant term is added in quadrature in the resolution. The overall resolution of the electromagnetic calorimeter of the D0 detector [13] ($\approx 0.15/\sqrt{E}$) is better than that of the CDF detector. Smearing effects are therefore less pronounced if the D0 parametrization for σ/E is used.

The SM parameters used in our calculations are $\alpha = \alpha(m_Z^2) = \frac{1}{128}$, $\alpha_s(m_Z^2) = 0.12$ (Ref. [14]), $m_Z = 91.1$ GeV, and $\sin^2\theta_W = 0.23$. For the parton distribution functions we use the Harriman-Martin-Roberts-Stirling set B [HMRS(B)] [15] with the scale Q^2 given by the parton center-of-mass energy squared, $\hat{s}$, unless stated otherwise.

B. Basic properties of the cross-section ratios

Using the results obtained in Refs. [1,2] it is straightforward to calculate the cross-section ratios (1.2)–(1.5) within the SM. If the ratios are considered as a function of the minimum transverse momentum of the photon $p_T^{\min}(\gamma)$ or the minimum weak-boson–photon-invariant mass $m_{\min}$, they reflect information carried by the $p_T(\gamma)$ and $m_{V\gamma}$ ($V = W, Z$) distributions. In the following we shall therefore study the cross-section ratios listed in Eqs. (1.2)–(1.5) as a function of these parameters. We shall also investigate in detail how the ratios are influenced by the cuts imposed on the final-state particles.

Figure 1(a) shows $\mathcal{R}_{\gamma,l}$ at the Fermilab Tevatron as a function of $p_T^{\min}(\gamma)$ for the cuts summarized in Eqs. (2.4)–(2.7). The ratio of $Z\gamma$ to $W^{\pm}\gamma$ cross sections (solid line) is seen to increase rapidly with the minimum photon transverse momentum from $\mathcal{R}_{\gamma,l} \approx 0.3$ at $p_T^{\min}(\gamma) = 10$ GeV to $\mathcal{R}_{\gamma,l} \approx 1.2$ at $p_T^{\min}(\gamma) = 200$ GeV. This is in sharp contrast to the ratio

$$\mathcal{R}_{j,l} = \frac{B(Z \to l^+ l^-)\sigma(Z_j)}{B(W \to l\nu)\sigma(W^{\pm} j)} , \tag{2.10}$$

which is shown versus the minimum jet transverse momentum $p_T^{\min}(j)$ for the same cuts [with the photon replaced by the jet in Eq. (2.4)] by the dashed line in Fig. 1(a). $\mathcal{R}_{j,l}$ remains in the range from 0.10 to 0.15 over the whole range of $p_T^{\min}(j)$ considered. The slight increase with the minimum jet transverse momentum is due to the different x behavior of the up- and down-type quark distribution functions. The ratio of Zj to $W^{\pm}j$ cross sections is thus very similar to $\mathcal{R}_l$ [see Eq. (1.1)], with the Zj production rate suppressed by approximately a factor 10 with respect to the $W^{\pm}j$ cross section. On the other hand, the $Z\gamma$ production rate is at most a factor 3 smaller than the $W^{\pm}\gamma$ cross section in the SM. At large photon transverse momenta, the rates for $W^{\pm}\gamma$ and $Z\gamma$ production are similar in magnitude.

The enhancement of the $Z\gamma$ cross section relative to the $W^{\pm}\gamma$ production rate can be understood as a consequence of the radiation zero present in the SM $q\bar{q}' \to W\gamma$ matrix elements [9], which suppresses $W\gamma$ production. For $u\bar{d} \to W^+\gamma$ ($d\bar{u} \to W^-\gamma$) all contributing helicity amplitudes vanish for $\cos\Theta = -\frac{1}{3}$ ($+\frac{1}{3}$), where Θ is the angle between the quark and the photon in the parton center-of-mass frame. As a result, the photon rapidity distribution $d\sigma/dy_\gamma^*$ in the $W\gamma$ rest frame develops a dip at zero rapidity when one sums over the W charges [1,6], thus reducing the cross section in the central rapidity re-

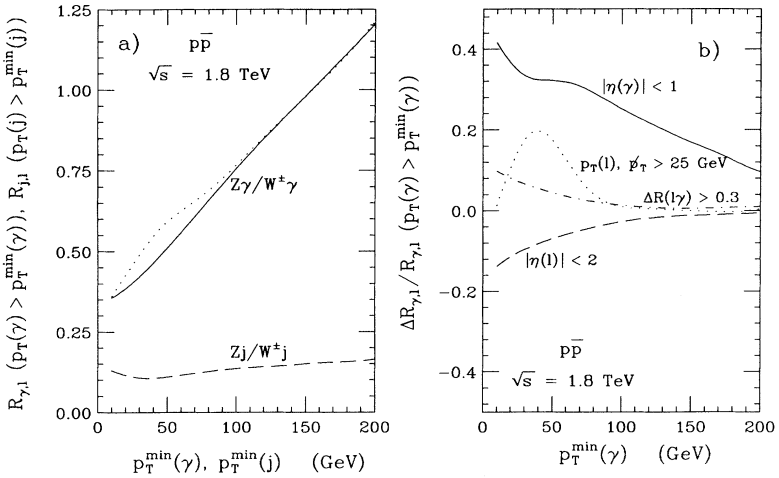

FIG. 1. (a) The ratio $\mathcal{R}_{\gamma,l}=B(Z\to l^+l^-)\sigma(Z\gamma)/B(W\to l\nu)\sigma(W^{\pm}\gamma)$ as a function of the minimum transverse momentum of the photon, $p_T^{\min}(\gamma)$, at the Tevatron for the cuts summarized in Eqs. (2.4)–(2.7) (solid line). The dashed line shows the corresponding ratio of Zj to $W^{\pm}j$ cross sections $\mathcal{R}_{j,l}$ [see Eq. (2.10)] versus $p_T^{\min}(j)$. The dotted line, finally, gives the result of $\mathcal{R}_{\gamma,l}$ for $p_T(l)$, $\not{p}_T > 25$ GeV, instead of the value listed in Eq. (2.4). (b) Sensitivity of $\mathcal{R}_{\gamma,l}$ at the Tevatron to the cuts imposed. The variation of the cross-section ratio, normalized to $\mathcal{R}_{\gamma,l}$ obtained for the cuts of Eq. (2.4), is shown versus $p_T^{\min}(\gamma)$. Only one cut at a time is varied.

gion. In contrast, there is no radiation zero present in $Z\gamma$ production, and the y_γ^* distribution peaks at $y_\gamma^*=0$ for $q\bar{q}\to Z\gamma$. For increasing photon transverse momenta, events become more central in rapidity. The reduction of the $W^{\pm}\gamma$ cross section for small rapidities originating from the radiation zero thus becomes more pronounced at high $p_T(\gamma)$. This causes the photon transverse momentum distribution of $q\bar{q}'\to W^{\pm}\gamma$ to fall significantly faster than the $p_T(\gamma)$ spectrum of $q\bar{q}\to Z\gamma$, which immediately translates into a sharp increase of $\mathcal{R}_{\gamma,l}$ with $p_T^{\min}(\gamma)$.

As mentioned before, the cuts of Eqs. (2.4)–(2.7) have been used in order to obtain $\mathcal{R}_{\gamma,l}$ shown in Fig. 1(a). It is important to know how the slope of $\mathcal{R}_{\gamma,l}$ versus $p_T^{\min}(\gamma)$ changes if the geometrical acceptances are varied. In Fig. 1(b), we display the variation of the cross-section ratio, normalized to the ratio obtained with the cuts of Eqs. (2.4)–(2.7), $\Delta\mathcal{R}_{\gamma,l}/\mathcal{R}_{\gamma,l}$, if these cuts are changed. Only one parameter is varied at a time. The sensitivity of $\mathcal{R}_{\gamma,l}$ to the cuts imposed in general decreases for increasing values of $p_T^{\min}(\gamma)$. Because of the radiation zero, the $W^{\pm}\gamma$ cross section is reduced more significantly than the $Z\gamma$ production rate, and $\mathcal{R}_{\gamma,l}$ increases, if the photon is required to be more central. This is illustrated by the solid line in Fig. 1(b), which shows the variation of $\mathcal{R}_{\gamma,l}$ if the pseudorapidity cut is changed from $|\eta(\gamma)|<3$ to $|\eta(\gamma)|<1$. The shoulder in the region between $p_T^{\min}(\gamma)\approx 30$ GeV and $p_T^{\min}(\gamma)\approx 70$ GeV can also be traced back to the radiation zero. For small values of the photon transverse momentum, the $\eta(\gamma)$ distribution is very flat in the $W^{\pm}\gamma$ case. At large $p_T(\gamma)$, the photon rapidity spectrum develops a slight dip at $\eta(\gamma)=0$ qualitatively similar to that in $d\sigma/dy_\gamma^*$. This leads to a shoulder in $\Delta\mathcal{R}_{\gamma,l}/\mathcal{R}_{\gamma,l}$ if the photon rapidity cut is reduced from $|\eta(\gamma)|<3$ to $|\eta(\gamma)|<1$. If the photon rapidity range is reduced even further, this shoulder progresses into a local maximum, located at $p_T^{\min}(\gamma)\approx 50$ GeV. On the other hand, a more stringent rapidity cut on the charged lepton pseudorapidity of $|\eta(l)|<2$ slightly reduces the cross-section ratio (dashed line). Changes in the lepton photon separation affect $\mathcal{R}_{\gamma,l}$ very little, as demonstrated by the dot-dashed line in Fig. 1(b).

The dotted line in Fig. 1(b), finally, shows the effect of increasing the $p_T(l)$ and $\not{p}_T$ cuts from 15 to 25 GeV. It exhibits an interesting structure in the region around $p_T^{\min}(\gamma)=m_W/2\approx 40$ GeV, where m_W is the W boson mass, which originates from the difference in the coupling of the leptons to W and Z bosons, and the Jacobian peak in the lepton p_T distribution. Because of the $V-A$ coupling of the leptons to the W boson, the charged lepton tends to be emitted in the direction of the parent W, thus picking up most of its momentum. Hence, the $p_T(l)$ distribution is significantly harder than the $\not{p}_T$ spectrum in $W^{\pm}\gamma$ production, whereas the transverse momentum distributions of the leptons in $Z\gamma$ production, as a result of the almost pure axial vector coupling of the charged leptons to the Z boson, almost coincide. Increasing the $\not{p}_T$ and $p_T(l)$ cuts from 15 to 25 GeV therefore reduce the $W^{\pm}\gamma$ cross section more than the $Z\gamma$ production rate, leading to an increase of $\mathcal{R}_{\gamma,l}$. In the region $p_T(\gamma)\gtrsim m_W/2$, the photon tends to recoil against (one of) the charged lepton(s). Because of the Jacobian peak in the $p_T(l)$ distribution, the sensitivity of $\mathcal{R}_{\gamma,l}$ is strongly enhanced around $p_T^{\min}(\gamma)=40$ GeV. In the cross-section ratio, the effect described above leads to a rather well-defined kink in $\mathcal{R}_{\gamma,l}$ versus the minimum photon transverse momentum at $p_T^{\min}(\gamma)\approx m_W/2$, as demonstrated by the dotted line in Fig. 1(a). At large values of $p_T^{\min}(\gamma)$, $\mathcal{R}_{\gamma,l}$ is almost independent of the cuts imposed on the final-state fermions. This ensures that the steep rise of $\mathcal{R}_{\gamma,l}$ with $p_T^{\min}(\gamma)$ is not an artifact of the specific set of cuts applied.

Although we have varied only one cut at a time, the curves in Fig. 1(b) correctly reflect the global sensitivity of $\mathcal{R}_{\gamma,l}$ to the cuts imposed. For example, changing the lepton rapidity cut from $|\eta(l)|<3.5$ to $|\eta(l)|<2$, and the $p_T(l)$ and $\not{p}_T$ cut from 15 to 25 GeV at the same time, gives a result for $\Delta\mathcal{R}_{\gamma,l}/\mathcal{R}_{\gamma,l}$ which is quite similar to that represented by the dotted line in Fig. 1(b). For increasing lepton transverse momenta, events are automatically more central in rapidity. A more stringent rapidity cut in addition to an increased p_T cut therefore changes

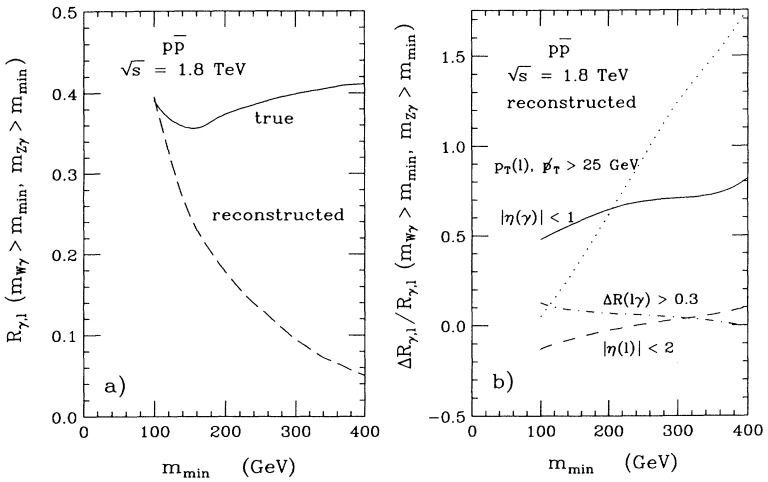

FIG. 2. (a) The ratio $\mathcal{R}_{\gamma,l}$ as a function of the minimum weak-boson–photon-invariant mass, $m_{\min}$, at the Tevatron for the cuts summarized in Eqs. (2.4)–(2.7). The solid line shows the ratio for the true $W\gamma$ invariant mass, whereas the dashed line gives the result if both solutions of the reconstructed longitudinal neutrino momentum are used with equal probabilities. (b) Sensitivity of $\mathcal{R}_{\gamma,l}$ at the Tevatron to the cuts imposed. The variation of the cross-section ratio, normalized to $\mathcal{R}_{\gamma,l}$ obtained for the cuts of Eq. (2.4), is shown versus $m_{\min}$. Only one cut at a time is varied.

the result only slightly.

The cross-section ratio $\mathcal{R}_{\gamma,l}$ as a function of the minimum invariant mass of the weak-boson–photon system, $m_{\min}$, for Fermilab Tevatron energies and the cuts of Eqs. (2.4)–(2.7) (solid line) is shown in Fig. 2(a). Because of threshold effects originating from the W/Z mass difference, $\mathcal{R}_{\gamma,l}$ drops first, before it starts to slowly rise. For most $W^{\pm}\gamma$ events with large $W\gamma$ invariant mass, the photon transverse momentum is fairly small, whereas $|\eta(\gamma)|$ is large. The radiation zero therefore does not manifest itself in $\mathcal{R}_{\gamma,l}$ if the cross-section ratio is considered as a function of $m_{\min}$.

At hadron colliders the $W\gamma$ invariant mass cannot be determined unambiguously because the neutrino from the W decay is not observed. If the transverse momentum of the neutrino is identified with the missing p_T of a given $W\gamma$ event, the unobservable longitudinal neutrino momentum can be reconstructed, albeit with a twofold ambiguity, by imposing the constraint that the neutrino and the charged lepton four-momenta combine to form the W rest mass [18]. On an event-by-event basis it is impossible to determine which of the two solutions corresponds to the actual neutrino longitudinal momentum. In the following we therefore use both solutions with equal probability when we consider cross-section ratios as a function of the $W\gamma$ invariant mass. This is the most conservative approach possible. The cross-section ratio $\mathcal{R}_{\gamma,l}$ for the reconstructed $W\gamma$ invariant mass is shown by the dashed line in Fig. 2(a). Only in the threshold region are the ratios for the true and reconstructed mass similar.

Figure 2(b) displays the variation of $\mathcal{R}_{\gamma,l}$ versus $m_{\min}$, using the reconstructed $W\gamma$ invariant mass, if the cuts of Eqs. (2.4)–(2.7) are changed, normalized to the cross-section ratio obtained with these cuts. As demonstrated by the dashed and dash-dotted curves, a more stringent rapidity cut on the charged leptons and a less severe separation cut have little influence on the cross-section ratio. Changes in the transverse momentum and photon rapidity cuts, on the other hand, have a larger effect. If the $p_T(l)$ and $\not{p}_T$ cut of Eq. (2.4) is increased to 25 GeV, the relative change in $\mathcal{R}_{\gamma,l}$ grows very rapidly with $m_{\min}$ (dotted line). Increasing the minimum lepton p_T selects a phase-space region where the two solutions of the longi-

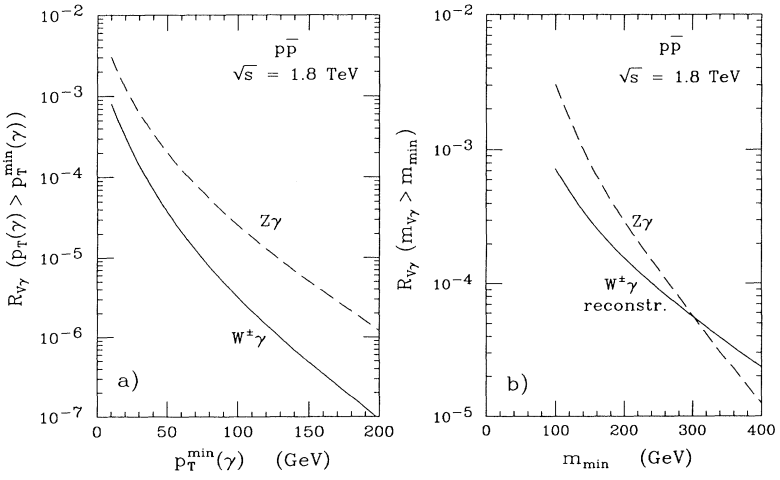

FIG. 3. The ratios $\mathcal{R}_{W\gamma}=\sigma(W^{\pm}\gamma)/\sigma(W^{\pm})$ (solid line) and $\mathcal{R}_{Z\gamma}=\sigma(Z\gamma)/\sigma(Z)$ (dashed line) (a) as a function of the minimum photon transverse momentum, $p_T^{\min}(\gamma)$, and (b) as a function of the minimum weak-boson–photon-invariant mass, $m_{\min}$, at the Tevatron. The cuts summarized in Eqs. (2.4)–(2.7) are imposed.

tudinal neutrino momentum tend to be closer together, so that $\mathcal{R}_{\gamma,l}$ resembles more closely the cross-section ratio obtained for the true $W\gamma$ invariant mass. Reducing the photon rapidity range covered increases the cross-section ratio by 50–70 % (solid line).

The results presented in Figs. 1(b) and 2(b) have been based on the lowest-order matrix elements of the contributing processes. As a result, the $W\gamma$ and $Z\gamma$ system is produced with zero transverse momentum. Higher-order QCD corrections give the $W\gamma/Z\gamma$ system a finite p_T, and thus may change how the cross-section ratio is affected when the $p_T(l)$ and $\not{p}_T$ cuts are varied. In order to take these effects properly into account, a complete calculation of the $W\gamma/Z\gamma$ transverse momentum distribution, including soft gluon resummation effects, is needed. At present, such a calculation is not available. However, one expects that the shapes of the $W\gamma$ and $Z\gamma$ transverse momentum distributions are similar to those of the W and Z boson p_T distributions. To roughly estimate how our predictions may change if the finite p_T of the weak-boson–photon system is taken into account, we have recalculated $\Delta\mathcal{R}_{\gamma,l}/\mathcal{R}_{\gamma,l}$, smearing the transverse momentum components of the final-state particles using the experimental p_T distribution of the W boson [17]. Possible differences in the shapes of $d\sigma/dp_T(W\gamma)$ and $d\sigma/dp_T(Z\gamma)$, and the sensitivity to details of the p_T spectrum, are simulated by using different fits to the observed W transverse momentum distribution. Each fit, appropriately normalized, is then identified with one of the transverse momentum distributions. The nonzero transverse momentum of the $W\gamma/Z\gamma$ system turns out to shift the dotted curves in Figs. 1(b) and 2(b) by typically a few percent. The shapes of the curves, however, remain almost unchanged.

So far, we have only considered the ratio of $Z\gamma$ to $W^{\pm}\gamma$ cross sections for Z decays into charged leptons, $\mathcal{R}_{\gamma,l}$. The cuts of Eqs. (2.6) and (2.7) efficiently suppress photon radiation from final-state leptons, and for equal photon p_T and rapidity cuts

$$\mathcal{R}_{\gamma,\nu}\approx\frac{B(Z\rightarrow\bar{\nu}\nu)}{B(Z\rightarrow l^+l^-)}\mathcal{R}_{\gamma,l}\approx 6\mathcal{R}_{\gamma,l}\ . \tag{2.11}$$

The basic properties of $\mathcal{R}_{\gamma,\nu}$ and $\mathcal{R}_{\gamma,l}$ are thus the same. In particular, $\mathcal{R}_{\gamma,\nu}$ also rises steeply with the minimum photon p_T, reflecting the radiation zero present in $W\gamma$ production in the SM.

The lowest-order prediction for $\mathcal{R}_{V\gamma}$ ($V=W,Z$) at the Fermilab Tevatron is shown in Fig. 3, using the cuts summarized in Eqs. (2.4)–(2.7). The solid lines give $\mathcal{R}_{W\gamma}$, whereas the dashed curves display the corresponding ratio for the $Z\gamma$ case. In order to calculate the Z boson cross section, $\sigma(Z)$, in $\mathcal{R}_{Z\gamma}$, we have assumed the lepton pair invariant mass to be in the range $65<m_{ll}\ll 115$ GeV. Photon exchange contributions and finite Z width effects are fully included in our calculation. Figure 3(a) shows the two ratios versus $p_T^{\min}(\gamma)$. Because of the radiation zero present in the SM, $\mathcal{R}_{W\gamma}$ is considerably smaller than $\mathcal{R}_{Z\gamma}$, and drops faster with increasing values of the minimum photon p_T. In Fig. 3(b), the cross-section ratios are plotted versus the minimum weak-boson–photon-invariant mass $m_{\min}$. As a result of the twofold ambiguity in the reconstruction of the longitudinal neutrino momentum, $\mathcal{R}_{W\gamma}$ decreases more slowly with $m_{\min}$ than $\mathcal{R}_{Z\gamma}$. The shape of $\mathcal{R}_{V\gamma}$ versus $p_T^{\min}(\gamma)$ and $m_{\min}$ changes only very little if the cuts on the final-state leptons are varied. The cross-section ratios typically vary by 10–30 %. For small values of $p_T^{\min}(\gamma)$ and $m_{\min}$ the changes in the cross sections cancel almost exactly in the ratio.

C. Theoretical and systematic uncertainties

Higher-order QCD corrections, and the choice of the parametrization of the parton distribution functions and the factorization scale Q^2, are the premier sources of uncertainties in the calculation of cross sections in hadronic collisions. It is therefore vital to investigate their impact on the cross-section ratios (1.2)–(1.5). The sensitivity of

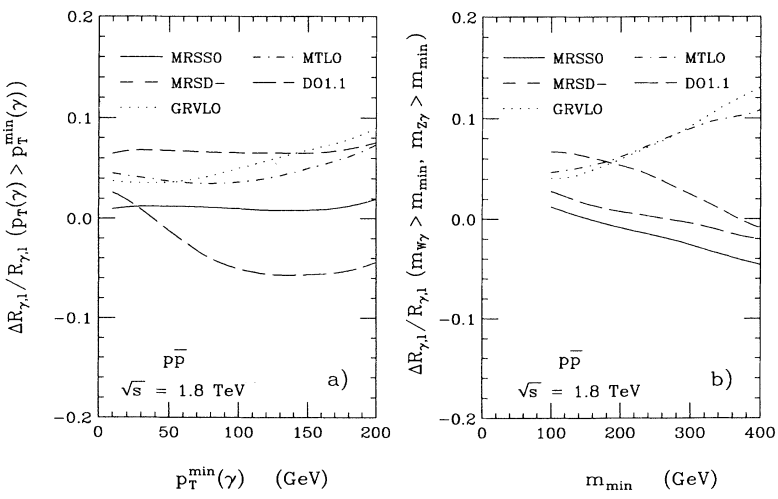

FIG. 4. Dependence of $\mathcal{R}_{\gamma,l}$ on the parametrization of the parton structure functions. The variation $\Delta\mathcal{R}_{\gamma,l}$, normalized to $\mathcal{R}_{\gamma,l}$ obtained with the HMRS(B) parametrization, is shown (a) versus $p_T^{\min}(\gamma)$ and (b) versus $m_{\min}$ for five representative parametrizations. The cuts used are summarized in Eqs. (2.4)–(2.7).

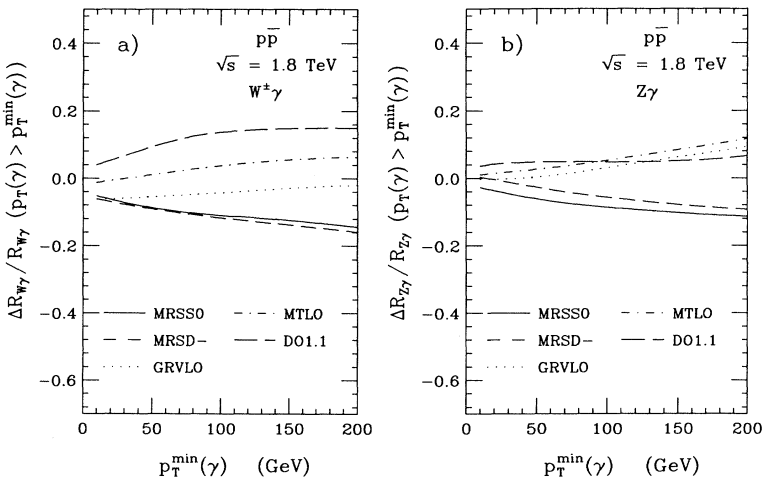

FIG. 5. Dependence of (a) $\mathcal{R}_{W\gamma}$ and (b) $\mathcal{R}_{Z\gamma}$ on the parametrization of the parton structure functions. The variation of the cross-section ratios is shown versus $p_T^{\min}(\gamma)$ for five representative fits, normalized to the cross-section ratio obtained with the HMRS(B) parametrization. The cuts imposed are summarized in Eqs. (2.4)–(2.7).

the ratios to the parametrization of the parton distribution functions is illustrated in Figs. 4 and 5 for five representative sets: the Martin-Roberts-Stirling set S_0 [MRS(S_0)] and MRS(D_) distributions of Ref. [18], the Glück-Reya-Vogt set LO [GRV(LO)] [19], the Morfin-Tung set LO [MT(LO)] [20], and the Duke-Owens set 1.1 [DO(1.1)] [21] parametrization. The MRS(S_0) and MRS(D_) sets take into account new New Muon Collaboration (NMC) [22] and Chicago-Columbia-Fermilab-Rochester (CCFR) [23] Collaboration data which suggest valence and sea quark distributions at low x which lead to considerably larger cross sections than previous fits. Figure 4 shows the variation of $\mathcal{R}_{\gamma,l}$ versus $p_T^{\min}(\gamma)$ [Fig. 4(a)] and $m_{\min}$ [Fig. 4(b)], normalized to the cross-section ratio obtained with the HMRS(B) set of distribution functions. Figure 5 displays $\Delta\mathcal{R}_{W\gamma}/\mathcal{R}_{W\gamma}$ [Fig. 5(a)] and $\Delta\mathcal{R}_{Z\gamma}/\mathcal{R}_{Z\gamma}$ versus $p_T^{\min}(\gamma)$ [Fig. 5(b)].

Although the $Z\gamma$ and $W^{\pm}\gamma$ total cross sections vary individually by up to 25% with the parametrization of the parton distributions, $\mathcal{R}_{\gamma,l}$ is found by be very stable. For $\mathcal{R}_{\gamma,l}$ as a function of $p_T^{\min}(\gamma)$ ($m_{\min}$), the changes are at most 8% (13%) in magnitude for the parametrizations used (see Fig. 4). $\mathcal{R}_{W\gamma}$ and $\mathcal{R}_{Z\gamma}$ are somewhat more sensitive. Here the ratios vary by up to 18 and 12 %, respectively, if considered as a function of the minimum photon transverse momentum (see Fig. 5). The variation of $\mathcal{R}_{V\gamma}$ ($V=W,Z$) versus $m_{\min}$ with the parametrization of the parton distribution function is qualitatively and quantitatively similar to that of $\mathcal{R}_{\gamma,l}$ and is therefore not shown.

The dependence of the cross-section ratios on the factorization scale Q^2 in the parton distribution functions is illustrated in Fig. 6. In this figure we show the variation of the cross-section ratios, normalized to the corresponding ratio obtained with $Q^2=\hat{s}$, for $Q^2=m_W^2$ (solid lines) and $Q^2=100m_W^2$ (dashed lines) versus $p_T^{\min}(\gamma)$. By choosing these two rather extreme values, we obtain a fairly conservative estimate of how strongly the cross-section ratios depend on the choice of Q^2. In tree-level calculations, one usually chooses a typical energy scale of the hard scattering process, such as the parton center-of-

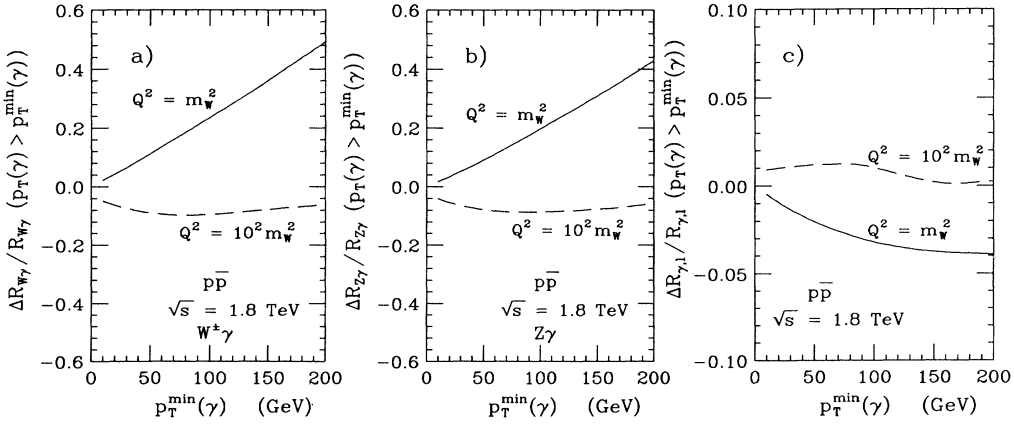

FIG. 6. Dependence of (a) $\mathcal{R}_{W\gamma}$, (b) $\mathcal{R}_{Z\gamma}$, and (c) $\mathcal{R}_{\gamma,l}$ on the choice of the factorization scale Q^2 in the parton distribution functions versus $p_T^{\min}(\gamma)$. The variation of the cross-section ratios with Q^2 is shown for $Q^2=m_W^2$ (solid lines) and $Q^2=100m_W^2$ (dashed lines), normalized to the cross-section ratio obtained with $Q^2=\hat{s}$. The cuts used are summarized in Eqs. (2.4)–(2.7).

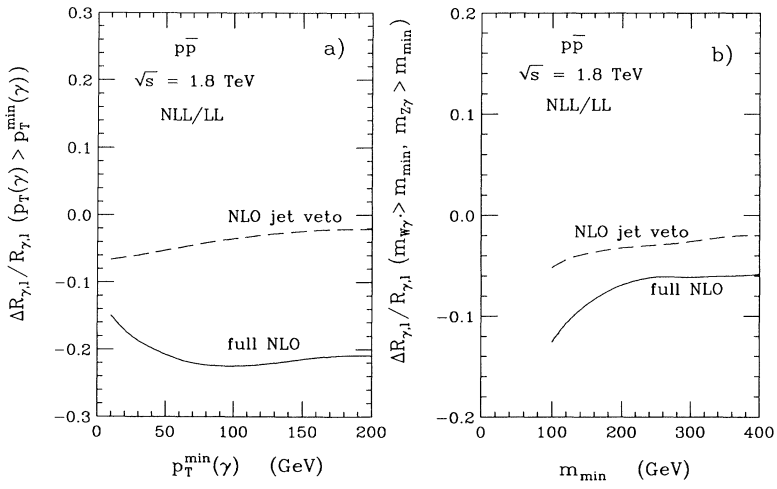

FIG. 7. Sensitivity of (a) $\mathcal{R}_{\gamma,l}$ versus $p_T^{\min}(\gamma)$ and (b) $\mathcal{R}_{\gamma,l}$ versus $m_{\min}$ to higher-order QCD corrections. The variation of the cross-section ratio, normalized to the result obtained in the Born [leading log (LL)] approximation, is shown for the full next-to-leading log QCD corrections (solid lines), and for the zero-jet requirement of Eq. (2.14) (dashed lines). The cuts imposed are listed in Eqs. (2.12) and (2.13).

mass energy squared, $\hat{s}$, for Q^2. If the cross-section ratios are calculated to all orders in α_s, the result is expected to be independent of Q^2.

For small values of the minimum transverse momentum of the photon and the weak-boson–photon-invariant mass, all cross-section ratios are quite insensitive to variations in Q^2. At large $p_T^{\min}(\gamma)$, however, the changes can be quite large for $\mathcal{R}_{W\gamma}$ and $\mathcal{R}_{Z\gamma}$, as illustrated by the solid lines in Figs. 6(a) and 6(b). The variations of the individual cross sections, however, cancel to a very good approximation in $\mathcal{R}_{\gamma,l}$ [Fig. 6(c)]. For $Q^2=100m_W^2$, the changes in the cross-section ratios with respect to $Q^2=\hat{s}$ are always smaller than 10%. Results similar to those shown in Fig. 6 are also obtained for $\mathcal{R}_{W\gamma}$ and $\mathcal{R}_{Z\gamma}$ as a function of $m_{\min}$. $\mathcal{R}_{\gamma,l}$ is somewhat more sensitive to the choice of Q^2 if considered as a function of $m_{\min}$ than the $Z\gamma$ to $W^{\pm}\gamma$ cross-section ratio versus $p_T^{\min}(\gamma)$ shown in Fig. 6(c).

The sensitivity of $\mathcal{R}_{W\gamma}$ and $\mathcal{R}_{Z\gamma}$ to the choice of Q^2 is expected to be reduced if next-to-leading log (NLL) QCD corrections are taken into account. NLL QCD corrections to $q\bar{q}\to Z\gamma$ and $q\bar{q}'\to W\gamma$ have been calculated recently in the framework of the SM in the limit of a stable, on-shell W/Z boson [7,8]. Naively one might expect that the cross-section ratios of Eqs. (1.2)–(1.5) change very little if higher-order QCD corrections are incorporated, similar to the ratio of $W^{\pm}$ and Z cross sections, $\mathcal{R}_l$, of Eq. (1.1) (Ref. [24]). Using the results of Refs. [8,25], we have investigated the influence of NLL QCD corrections on the cross-section ratios. Our results are shown in Figs. 7 and 8. In order to perform a meaningful comparison, the cross section for $q\bar{q}'\to W^{\pm}\gamma$ and $q\bar{q}\to Z\gamma$ in the Born approximation is also calculated in the limit of a stable, on-shell W/Z boson. To roughly simulate detector response, the following transverse momentum and rapidity cuts are imposed:

$$p_T(\gamma)>10\ \text{GeV},\quad |\eta(\gamma)|<1,\quad \text{and}\quad |y(V)|<2.5\ . \tag{2.12}$$

Here, $y(V)$ ($V=W,Z$) is the W/Z rapidity. We also require the photon to be isolated by imposing a cut on the total hadronic energy in a cone of size $\Delta R=0.7$ about the direction of the photon of

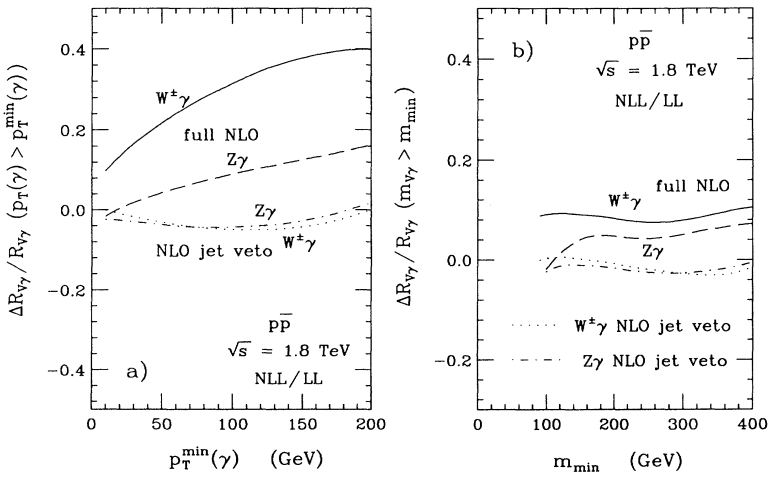

FIG. 8. Sensitivity of (a) $\mathcal{R}_{V\gamma}$ versus $p_T^{\min}(\gamma)$ and (b) $\mathcal{R}_{V\gamma}$ versus $m_{\min}$ ($V=W,Z$) to higher-order QCD corrections. The variation of the cross-section ratio, normalized to the result obtained in the Born [leading log (LL)] approximation, is shown for the full next-to-leading log QCD corrections and for the zero-jet requirement of Eq. (2.14). The cuts used are summarized in Eqs. (2.12) and (2.13).

$$\sum_{\Delta R<0.7} E_{\rm had} < 0.15 E_{\gamma} \ , \tag{2.13}$$

where E_{γ} is the photon energy. This requirement strongly reduces photon bremsstrahlung from final-state quarks and gluons.

The results shown in Figs. 7 and 8 demonstrate that, in contrast with $\mathcal{R}_l$, the NLL QCD corrections to the cross sections only partially cancel in $\mathcal{R}_{\gamma,l}$, $\mathcal{R}_{W\gamma}$, and $\mathcal{R}_{Z\gamma}$, in particular when these cross-section ratios are considered as a function of $p_T^{\rm min}(\gamma)$. Since the QCD corrections tend to wash out the SM radiation zero in $q\bar{q}' \to W^{\pm}\gamma$, $\mathcal{R}_{W\gamma}$ is significantly more sensitive to NLL order effects than $\mathcal{R}_{Z\gamma}$ [see Fig. 8(b)]. At large values of $p_T^{\rm min}(\gamma)$, $\mathcal{R}_{W\gamma}$ increases by as much as 40% if QCD corrections are included. On the other hand, $\mathcal{R}_{\gamma,l}$ is reduced by typically 15–20 % by $O(\alpha_s)$ corrections [solid line in Fig. 7(a)].

Higher-order QCD effects are known to change the shapes of the $p_T(\gamma)$ and invariant mass distributions in $W\gamma$ and $Z\gamma$ production [8]. This effect can be traced to the quark gluon fusion process $qg \to W\gamma q'$ and $qg \to Z\gamma q$, which carries an enhancement factor $\log^2[p_T^2(\gamma)/m_V^2]$ $(V=W,Z)$ at large values of $p_T(\gamma)$. This enhancement factor arises from the kinematic region where the photon is produced at large transverse momentum and recoils against the quark, which radiates a soft W/Z which is almost collinear to the quark [26]. The shape of the photon p_T distribution is therefore significantly affected by higher-order QCD corrections, and the corrections to the cross-section ratios as a function of $p_T^{\rm min}(\gamma)$ depend strongly on the minimum photon p_T. Since $O(\alpha_s)$ corrections result in a harder $p_T(\gamma)$ distribution, the corrections to the cross-section ratios grow with $p_T^{\rm min}(\gamma)$. The shape of the $Z\gamma$ and the reconstructed $W\gamma$ invariant-mass distribution, on the other hand, is only slightly affected by higher-order QCD corrections. Away from the threshold region, the corrections to the cross-section ratios as a function of $m_{\rm min}$ are approximately constant.

From the discussion above it is clear that the size of the $O(\alpha_s)$ QCD corrections to the cross-section ratios of Eqs. (1.2)–(1.5) can be significantly reduced by vetoing hard jets in the central rapidity region. Requiring

$$no \text{ jets with } p_T(j) > 10 \text{ GeV}, \quad |\eta(j)| < 2.5 \tag{2.14}$$

in the event, we obtain the results shown by the dashed line (dotted and dash-dotted lines) in Fig. 7 (Fig. 8). A "zero-jet" cut similar to that in Eq. (2.14) has been imposed in the CDF measurement of the ratio of W to Z cross sections, $\mathcal{R}_l$ [27], and the W mass measurement [28]. Imposing the jet veto of Eq. (2.14), reduces the corrections to the cross-section ratios from higher-order QCD effects to the few percent level in the $p_T^{\rm min}(\gamma)$ and $m_{\rm min}$ range studied.

The results shown in Figs. 7 and 8 have been obtained for on-shell W/Z bosons. No qualitative changes to these results are expected if decay correlations, finite W/Z width effects, and photon exchange diagrams are taken into account. At present, a calculation of NLL QCD corrections to both $W^{\pm}\gamma$ and $Z\gamma$ production, which fully takes into account these effects, does not exist.

As mentioned before, $\mathcal{R}_{\gamma,\nu}$ is approximately proportional to $\mathcal{R}_{\gamma,l}$ for the cuts imposed [see Eq. (2.11)]. The results shown in Figs. 4(a), 6(c), and 7(a) therefore apply also to $\mathcal{R}_{\gamma,\nu}$.

III. MEASURING THREE VECTOR BOSON COUPLINGS IN CROSS-SECTION RATIOS

A. $\mathcal{R}_{\gamma,l}$, $\mathcal{R}_{\gamma,\nu}$ and the standard model radiation zero

In Sec. II B, we have seen that the strong increase of the ratios of $Z\gamma$ to $W^{\pm}\gamma$ cross sections, $\mathcal{R}_{\gamma,l}$ and $\mathcal{R}_{\gamma,\nu}$, as a function of the minimum transverse momentum of the photon can be traced to the radiation zero which is present in the SM $q\bar{q}' \to W\gamma$ differential cross section. In the last section we have shown that $\mathcal{R}_{\gamma,l}$ and $\mathcal{R}_{\gamma,\nu}$ are quite insensitive to changes in the parametrization of the parton structure functions. Furthermore, at the tree level the two ratios vary little with a change of the factorization scale Q^2. Finally, when a central jet veto is imposed, the $O(\alpha_s)$ QCD corrections change $\mathcal{R}_{\gamma,l}$ and $\mathcal{R}_{\gamma,\nu}$ by only a few percent.

The steep rise of $\mathcal{R}_{\gamma,l}$ and $\mathcal{R}_{\gamma,\nu}$ with $p_T^{\rm min}(\gamma)$ in the framework of the SM as a signal of the radiation zero, combined with small systematic and theoretical uncertainties, make these quantities excellent tools to probe the three vector boson vertices. As we shall see below, anomalous $WW\gamma$ couplings tend to decrease the two ratios, in particular at large $p_T^{\rm min}(\gamma)$. Nonstandard $ZZ\gamma$ and $Z\gamma\gamma$ couplings, on the other hand, lead to an increase of $\mathcal{R}_{\gamma,l}$ and $\mathcal{R}_{\gamma,\nu}$ to values much larger than predicted by the SM. In contrast with other quantities which are sensitive to the radiation zero, $\mathcal{R}_{\gamma,l}$ is fairly simple to measure experimentally. The prospects for $\mathcal{R}_{\gamma,\nu}$ depend on how well the $p\bar{p} \to \gamma \not{p}_T$ signal can be isolated [2]. As we have mentioned before, the photon rapidity distribution $d\sigma/dy_{\gamma}^*$ in the $W\gamma$ center-of-mass system is a quantity which is sensitive to the radiation zero. The measurement of $d\sigma/dy_{\gamma}^*$ is complicated by the fact that the neutrino is not observed, which leads to a twofold ambiguity in the reconstruction of the $W\gamma$ center-of-mass system [16]. On an event-by-event basis it is impossible to decide which of the two solutions is the correct one. As a result, the radiation zero is partially washed out. On the other hand, the measurement of $\mathcal{R}_{\gamma,l}$ and $\mathcal{R}_{\gamma,\nu}$ versus $p_T^{\rm min}(\gamma)$ is relatively easy, and essentially involves only counting the number of $W^{\pm}\gamma$ and $Z\gamma$ events as a function of the minimum photon transverse momentum.

The ratio $\mathcal{R}_{\gamma,l}$ may also be very useful in observing the radiation zero at the CERN Large Hadron Collider (LHC) [pp collisions at $\sqrt{s}=15.4$ TeV (Ref. [29])] and the Superconducting Super Collider (SSC) (pp collisions at $\sqrt{s}=40$ TeV). At these center-of-mass energies the higher-order QCD corrections to $W^{\pm}\gamma$ production completely obscure the radiation zero in $d\sigma/dy_{\gamma}^*$ (Ref. [8]), even when a rather tight central jet veto is imposed [30]. The $O(\alpha_s)$ QCD corrections to $\mathcal{R}_{\gamma,l}$, on the other hand,

are found to be well under control if one requires that no jets with $p_T(j) > 50$ GeV and $|\eta(j)| < 3$ are present in the event.

The tree-level prediction of $\mathcal{R}_{\gamma,l}$ at hadron supercolliders as a function of the minimum photon transverse momentum is shown in Fig. 9. To simulate detector response, we have imposed the following set of cuts:

$$p_T(\gamma) > 100 \text{ GeV}, \quad |\eta(\gamma)| < 3 ,$$
$$p_T(l), \not{p}_T > 20 \text{ GeV}, \quad |\eta(l)| < 3 , \tag{3.1}$$
$$m_{ll} > 50 \text{ GeV}, \quad \Delta R(l\gamma) > 0.7 .$$

Energy mismeasurements in the detector were simulated by Gaussian smearing of the charged lepton and photon momenta using the expected resolution of the Solenoidal Detector Collaboration (SDC) [31].

At the LHC and SSC, $\mathcal{R}_{\gamma,l}$ grows with increasing values of $p_T^{\min}(\gamma)$, similar to the situation encountered for Fermilab Tevatron energies. Because of the smaller center-of-mass energy available at the LHC, $\mathcal{R}_{\gamma,l}$ rises faster than at SSC energies (solid line). For example, a minimum photon p_T of 1 TeV at LHC energies corresponds to $p_T^{\min}(\gamma) \approx 2.6$ TeV at $\sqrt{s} = 40$ TeV. For these values of $p_T^{\min}(\gamma)$, $\mathcal{R}_{\gamma,l}$ is approximately equal for both energies. The ratio of Zj to $W^{\pm}j$ cross sections, $\mathcal{R}_{j,l}$, on the other hand, stays approximately constant ($\mathcal{R}_{j,l} \approx 0.12$) over the entire range of $p_T^{\min}(j)$ values considered (dotted and dash-dotted lines). Therefore, $\mathcal{R}_{\gamma,l}$ reflects the radiation zero also at supercollider energies.

Compared to $\mathcal{R}_{V\gamma}$ ($V = W, Z$), $\mathcal{R}_{\gamma,l}$ and $\mathcal{R}_{\gamma,\nu}$ have the advantage of reflecting the SM radiation zero. Moreover, at the tree level, systematic and theoretical errors are significantly smaller for these cross-section ratios than for $\mathcal{R}_{V\gamma}$. On the other hand, because of the large total W and Z cross section, statistical errors are expected to be considerably smaller in $\mathcal{R}_{V\gamma}$. Furthermore, cancellations between anomalous $WW\gamma$ and $ZZ\gamma/Z\gamma\gamma$ couplings may occur in $\mathcal{R}_{\gamma,l}$ and $\mathcal{R}_{\gamma,\nu}$ (see below). This is not possible in $\mathcal{R}_{V\gamma} = \sigma(V\gamma)/\sigma(V)$. The various $W^{\pm}\gamma$ and $Z\gamma$ cross-section ratios listed in Eqs. (1.2)–(1.5) therefore yield complementary information on the structure of three vector boson vertices.

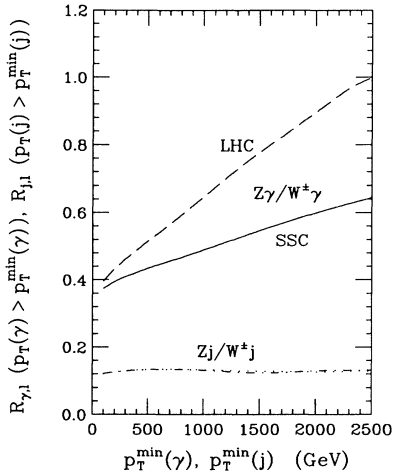

FIG. 9. The ratio $\mathcal{R}_{\gamma,l}$ as a function of the minimum transverse momentum of the photon, $p_T^{\min}(\gamma)$, at the LHC (dashed line) and SSC (solid line) for the cuts summarized in Eq. (3.1). The dotted and dash-dotted line show the corresponding ratio of Zj to $W^{\pm}j$ cross sections, $\mathcal{R}_{j,l}$, versus $p_T^{\min}(j)$.

B. Probing three vector boson vertices via cross-section ratios

We shall now discuss the impact of nonstandard three vector boson couplings on the $W^{\pm}\gamma$ and $Z\gamma$ cross-section ratios in more detail. The couplings of W and Z bosons to quarks and leptons are assumed to be given by the SM. We shall also assume that there are no nonstandard couplings of the $Z\gamma$ pair to two gluons [32]. The W and Z bosons entering the Feynman diagrams for $q\bar{q}' \to W\gamma$ and $q\bar{q} \to Z\gamma$ couple to essentially massless fermions, which ensures that effectively $\partial_\mu V^\mu = 0$ ($V = W, Z$). This together with gauge invariance of the on-shell photon restricts the tensor structure of the $WW\gamma$, $ZZ\gamma$, and $Z\gamma\gamma$ vertex to allow just four free parameters. The $WW\gamma$ vertex function for the process $q\bar{q}' \to W^{\pm}\gamma$ is then given by [33] (see Fig. 10) for notation)

$$\Gamma^{\alpha\beta\mu}_{W\gamma W}(q_1, q_2, P) = \mp \frac{1}{2} \left\{ (1+\kappa)(q_1 - q_2)^\mu g^{\alpha\beta} + \frac{\lambda}{m_W^2}(q_1 - q_2)^\mu (P^2 g^{\alpha\beta} - 2P^\alpha P^\beta) \right.$$
$$\left. - 4P^\beta g^{\mu\alpha} + 2(1+\kappa+\lambda)P^\alpha g^{\mu\beta} + 2(\tilde{\kappa}+\tilde{\lambda})\epsilon^{\mu\alpha\beta\rho} q_{2\rho} + \frac{\tilde{\lambda}}{m_W^2}(q_1 - q_2)^\mu \epsilon^{\alpha\beta\rho\sigma} P_\rho (q_1 - q_2)_\sigma \right\} . \tag{3.2}$$

The parameters κ ($\tilde{\kappa}$) and λ ($\tilde{\lambda}$) are related to the magnetic (electric) dipole moment μ_W (d_W) and the electric (magnetic) quadrupole moment Q_W ($\tilde{Q}_W$) of the W boson by

$$\mu_W = \frac{e}{2M_W}(1+\kappa+\lambda) , \tag{3.3a}$$

$$Q_W = -\frac{e}{m_W^2}(\kappa - \lambda) , \tag{3.3b}$$

$$d_W = \frac{e}{2m_W}(\tilde{\kappa}+\tilde{\lambda}) , \tag{3.3c}$$

$$\tilde{Q}_W = -\frac{e}{m_W^2}(\tilde{\kappa} - \tilde{\lambda}) . \tag{3.3d}$$

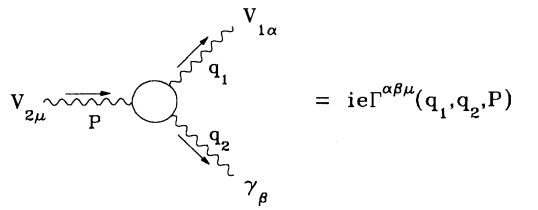

FIG. 10. Feynman rule for the general $V_1\gamma V_2$, $V_1=W,Z$, $V_2=W,Z,\gamma$ vertex. e is the charge of the proton.

While the κ and λ terms to not violate any discrete symmetries, the $\tilde{\kappa}$ and $\tilde{\lambda}$ terms are P odd and CP violating. Within the SM, at tree level,

$$\kappa=1,\quad \lambda=0\ ,$$
$$\tilde{\kappa}=0,\quad \tilde{\lambda}=0\ . \tag{3.4}$$

The CP-violating couplings $\tilde{\kappa}$ and $\tilde{\lambda}$ are constrained by measurements of the electric dipole moment of the neutron to be smaller than $\sim 10^{-3}$ in magnitude [34]. Therefore, they will not be discussed subsequently. The CP-conserving couplings κ and λ have been measured recently by the UA2 Collaboration in the process $p\bar{p}\rightarrow e^{\pm}\nu\gamma X$ at the CERN $p\bar{p}$ collider [35]:

$$\kappa=1^{+2.6}_{-2.2}\ \ (\text{for } \lambda=0)\ ,$$
$$\lambda=0^{+1.7}_{-1.8}\ \ (\text{for } \kappa=1)\ , \tag{3.5}$$

at the 68% C.L. The analysis of the 1988-1989 CDF $W\gamma$ (and $Z\gamma$) data is still in progress [36].

The most general anomalous $Z\gamma Z$ vertex function (see Fig. 10 for notation) is given by [37]

$$\Gamma^{\alpha\beta\mu}_{Z\gamma Z}(q_1,q_2,P)=\frac{P^2-q_1^2}{m_Z^2}\left\{h_1^Z(q_2^\mu g^{\alpha\beta}-q_2^\alpha g^{\mu\beta})+\frac{h_2^Z}{m_Z^2}P^\alpha[(P\cdot q_2)g^{\mu\beta}-q_2^\mu P^\beta]+h_3^Z\epsilon^{\mu\alpha\beta\rho}q_{2\rho}+\frac{h_4^Z}{m_Z^2}P^\alpha\epsilon^{\mu\beta\rho\sigma}P_\rho q_{2\sigma}\right\}\ , \tag{3.6}$$

where m_Z is the Z boson mass. The most general $Z\gamma\gamma$ vertex function can be obtained from Eq. (3.6) by the replacements

$$\frac{P^2-q_1^2}{m_Z^2}\rightarrow\frac{P^2}{m_Z^2} \tag{3.7}$$

and

$$h_i^Z\rightarrow h_i^\gamma,\quad i=1,\ldots,4\ .$$

Terms proportional to P^μ and q_1^α have been omitted in Eq. (3.6) since they do not contribute to the cross section. The overall factor $(P^2-q_1^2)$ in Eq. (3.6) is a result of Bose symmetry, whereas the factor P^2 in the $Z\gamma\gamma$ vertex function originates from electromagnetic gauge invariance. As a result the $Z\gamma\gamma$ vertex function vanishes identically if both photons are on shell [38]. All $ZZ\gamma$ and $Z\gamma\gamma$ couplings are C odd; h_1^V and h_2^V ($V=Z,\gamma$) violate CP. Combinations of h_3^V (h_1^V) and h_4^V (h_2^V) correspond to the electric (magnetic) dipole and magnetic (electric) quadrupole transition moment of the Z boson. At the tree level in the SM, all couplings h_i^V vanish. Presently, there are no limits on h_i^V from hadron collider experiments. LEP I data give only very loose constraints of $h_i^V\sim 10-100$ (Ref. [2]). Without loss of generality we have chosen the overall $WW\gamma$, $ZZ\gamma$, and $Z\gamma\gamma$ coupling constant to be

$$g_{WW\gamma}=g_{ZZ\gamma}=g_{Z\gamma\gamma}=e\ , \tag{3.8}$$

where e is the charge of the proton.

Tree-level unitarity restricts the $WW\gamma$, $ZZ\gamma$, and $Z\gamma\gamma$ couplings uniquely to their SM values at asymptotically high energies [39]. This implies that the $WW\gamma$ and $Z\gamma W$ couplings $a=\kappa-1,\ldots,\tilde{\lambda}$ and h_i^V have to be described by form factors $a(q_1^2,q_2^2,P^2)$ and $h_i^V(q_1^2,q_2^2,P^2)$ which vanish when q_1^2, q_2^2, or P^2 becomes large. Following Refs. [2,6], we shall use generalized dipole form factors of the form

$$a(m_W^2,0,\hat{s})=\frac{a_0}{(1+\hat{s}/\Lambda^2)^n} \tag{3.9a}$$

and

$$h_i^V(m_Z^2,0,\hat{s})=\frac{h_{i0}^V}{(1+\hat{s}/\Lambda^2)^n}\ . \tag{3.9b}$$

In order to guarantee unitarity, n must satisfy $n>\frac{1}{2}$ for $a=\Delta\kappa=\kappa-1$, $\tilde{\kappa},n>1$ for $a=\lambda,\tilde{\lambda}$ (Ref. [6]), and $n>\frac{3}{2}$ ($n>\frac{5}{2}$) for $h_{1,3}^V$ ($h_{2,4}^V$) (Ref. [2]). In Eq. (3.9) Λ represents the scale at which new physics becomes important in the weak boson sector. In the following, we chose $\Lambda=750$ GeV, $n=2$ for $WW\gamma$ couplings, and $n=3$ ($n=4$) for $h_{1,3}^V$ ($h_{2,4}^V$).

The influence of anomalous $WW\gamma$ couplings on the ratio of $Z\gamma$ to $W^{\pm}\gamma$ cross sections is shown in Fig. 11 for the cuts summarized in Eqs. (2.4)–(2.7). For presentational reasons we display the inverse cross-section ratio

$$\mathcal{R}_{\gamma,l}^{-1}=\frac{B(W\rightarrow l\nu)\sigma(W^{\pm}\gamma)}{B(Z\rightarrow l^+l^-)\sigma(Z\gamma)}\ . \tag{3.10}$$

The solid curves show the SM result. The error bars indicate the statistical errors, corresponding to the 68.3% confidence level (C.L.) interval, expected for an integrated luminosity of $\int\mathcal{L}dt=25$ pb^{-1} and considering only $W\rightarrow e\nu$ and $Z\rightarrow e^+e^-$ decays. If the muon final states of the weak boson decays are taken into account as well, the statistical errors may be significantly reduced. De-

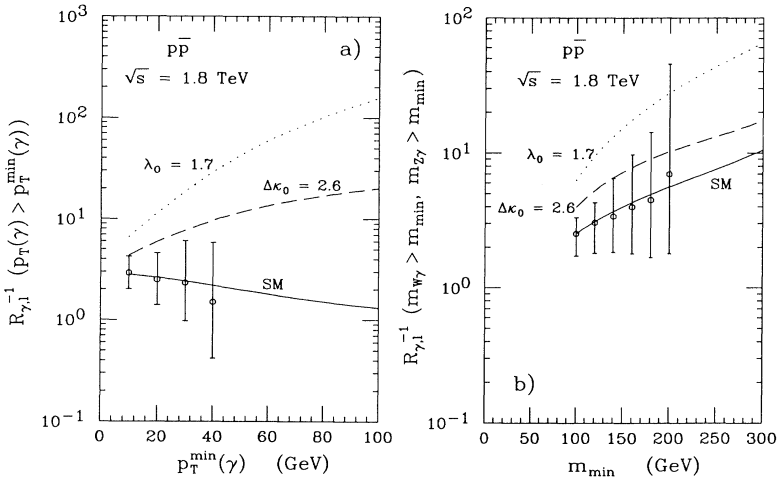

FIG. 11. The inverse cross-section ratio $\mathcal{R}_{\gamma,l}^{-1}$ at the Tevatron (a) versus $p_T^{\min}(\gamma)$ and (b) versus $m_{\min}$. The cuts imposed are listed in Eqs. (2.4)–(2.7). The curves are for the SM (solid), $\Delta\kappa_0=2.6$ (dashed), and $\lambda_0=1.7$ (dotted). A dipole form factor ($n=2$) with $\Lambda=750$ GeV is used to obtain the curves for nonstandard couplings. The error bars indicate the expected statistical errors for an integrated luminosity of 25 pb^{-1} for $W\to e\nu$ and $Z\to e^+e^-$ decays. Only one $WW\gamma$ coupling is varied at a time. All $ZZ\gamma$ and $Z\gamma\gamma$ couplings are assumed to vanish identically.

tails depend strongly on the rapidity coverage for muons, which is quite different for CDF [40] and D0 [13]. When estimating the errors of the cross-section ratios, care must be taken for large values of $p_T^{\min}(\gamma)$ and $m_{\min}$ where the number of events in both the numerator and denominator can be very small. To estimate the statistical errors in these regions, we have used the method described in Ref. [41]. For an integrated luminosity of $\int\mathcal{L}dt=100$ pb^{-1}, as foreseen by the end of 1994, the error bars in Fig. 11 and all subsequent figures are reduced by a factor 1.5–2. The dashed and dotted curves show $\mathcal{R}_{\gamma,l}$ for $\Delta\kappa_0=2.6$ and $\lambda_0=1.7$, the present UA2 68% C.L. limits on the *CP*-conserving $WW\gamma$ couplings [35]. Only one coupling is varied at a time. For the form factor parameters used ($n=2$ and $\Lambda=750$ GeV), the values of the two couplings are about a factor 5 and 4 below the unitarity bound, respectively [6]. The anomalous $ZZ\gamma$ and $Z\gamma\gamma$ couplings, h_{i0}^V, are assumed to be zero in Fig. 11. All numerical results shown in this section are obtained using the tree-level calculations of Refs. [1,2].

Since the anomalous terms in the helicity amplitudes grow like $\sqrt{\hat{s}}/m_W$ for $\Delta\kappa$ and $\hat{s}/m_W^2$ for λ, nonstandard $WW\gamma$ couplings lead to an excess of events at large values of the photon transverse momentum and the $W\gamma$ invariant mass. As a result, $\mathcal{R}_{\gamma,l}^{-1}$ is larger than in the SM if anomalous $WW\gamma$ couplings are present. Because of the radiation zero one expects $\mathcal{R}_{\gamma,l}^{-1}$ to fall with increasing $p_T^{\min}(\gamma)$ in the SM [see Fig. 11(a)]. For anomalous couplings, on the other hand, the inverse cross-section ratio rises very rapidly with the minimum photon transverse momentum.

Figure 11 shows that it should be possible to measure $\mathcal{R}_{\gamma,l}^{-1}$ for minimum photon transverse momenta up to 40 GeV, and values of $m_{\min}$ up to 200 GeV, with 25 pb^{-1}. Comparing Figs. 11(a) and 11(b) it is obvious that $\mathcal{R}_{\gamma,l}^{-1}$ as a function of $p_T^{\min}(\gamma)$ is more sensitive to anomalous couplings than the inverse cross-section ratio versus $m_{\min}$. The reduced sensitivity in $\mathcal{R}_{\gamma,l}^{-1}$ as a function of the minimum weak-boson–photon-invariant mass is mostly due to the ambiguity in the reconstructed longitudinal neutrino momentum, $p_{\nu L}$. As before, we have used both solutions for $p_{\nu L}$ with equal weight in Fig. 11(b). The sensitivity of $\mathcal{R}_{\gamma,l}^{-1}$ versus $m_{\min}$ would clearly improve if one could discriminate between the two solutions on a statistical basis. Finally, Fig. 11 demonstrates that the UA2 limits on $\Delta\kappa$ and λ can be considerably improved at the Fermilab Tevatron with an integrated luminosity of 25 pb^{-1}.

The impact of anomalous $ZZ\gamma$ couplings on $\mathcal{R}_{\gamma,l}$ is shown in Fig. 12 for $h_{30}^Z=1$ and $h_{40}^Z=0.075$. For the

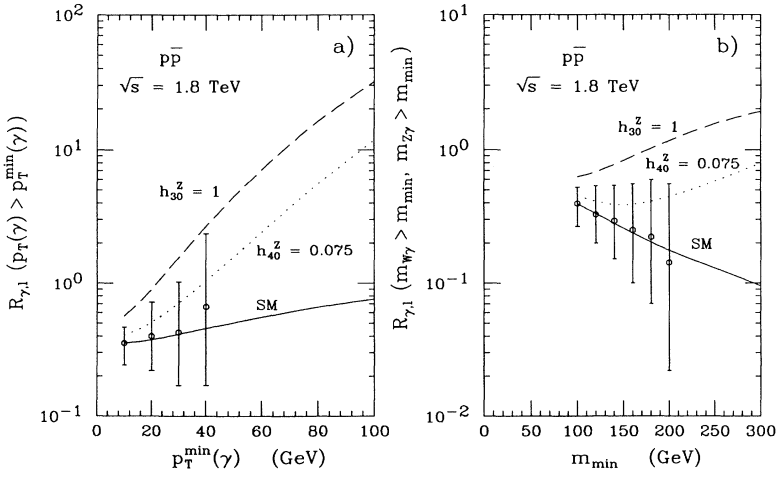

FIG. 12. The cross-section ratio $\mathcal{R}_{\gamma,l}$ at the Tevatron (a) versus $p_T^{\min}(\gamma)$ and (b) versus $m_{\min}$. The cuts used are summarized in Eqs. (2.4)–(2.7). The curves are for the SM (solid), $h_{30}^Z=1$ (dashed), and $h_{40}^Z=0.075$ (dotted). For the form factor parameters [see Eq. (3.9)] we assume $n=3$ ($n=4$) for h_{30}^Z (h_{40}^Z) with $\Lambda=750$ GeV. The error bars indicate the expected statistical errors for an integrated luminosity of 25 pb^{-1} for $W\to e\nu$ and $Z\to e^+e^-$ decays. Only one $ZZ\gamma$ coupling is varied at a time. Anomalous $WW\gamma$ and $Z\gamma\gamma$ couplings are assumed to vanish identically.

form factor parameters used [$n=3$ ($n=4$) for h_3^Z (h_4^Z), and $\Lambda=750$ GeV], these values are approximately a factor 2 below the limit allowed by unitarity [2]. The $WW\gamma$ and $Z\gamma\gamma$ vertex functions are assumed to have SM form in Fig. 12. For equal coupling strengths, the numerical results obtained for the $Z\gamma\gamma$ couplings h_3^γ and h_4^γ are about 20% below those obtained for h_3^Z and h_4^Z, in the region where anomalous coupling effects dominate over the SM cross section. Results for the *CP*-violating couplings $h_{1,2}^V$ ($V=Z,\gamma$) are virtually identical to those obtained for the same values of $h_{3,4}^V$. Anomalous $ZZ\gamma$ and $Z\gamma\gamma$ couplings are seen to increase $\mathcal{R}_{\gamma,l}$ dramatically, especially at large values of the minimum photon p_T. In contrast with the situation for anomalous $WW\gamma$ couplings, the sensitivity of $\mathcal{R}_{\gamma,l}$ to $ZZ\gamma/Z\gamma\gamma$ couplings is not degraded substantially if the ratio is considered as a function of $m_{\min}$ [see Fig. 12(b)].

For an integrated luminosity of 25 pb^{-1}, the sensitivity of $\mathcal{R}_{\gamma,l}$ to nonstandard three vector boson vertices is limited mostly by statistical errors. From the results of Sec. II C we estimate the systematic errors for $\mathcal{R}_{\gamma,l}$ to be approximately 10%. Due to the larger branching ratio of the decay $Z\to\bar{\nu}\nu$, the statistical error in the cross-section ratio of Eq. (1.3), $\mathcal{R}_{\gamma,\nu}$ is reduced by a factor 1.4–1.7. The cross-section ratio $\mathcal{R}_{\gamma,\nu}$ and its inverse are shown in Fig. 13 as a function of the minimum photon transverse momentum for the cuts summarized in Eqs. (2.4) and (2.7). The photon transverse momentum cut in Fig. 13 has been increased to $p_T(\gamma)>30$ GeV, in order to suppress backgrounds from $p\bar{p}\to\gamma j$, with the jet rapidity outside the range covered by the detector and thus "faking" missing transverse momentum, and two-jet production where one of the jets is misidentified as a photon while the other disappears through the beam hole [2]. Comparing Fig. 13 with Figs. 11(a) and 12(a), the increased sensitivity of $\mathcal{R}_{\gamma,\nu}$ to anomalous three vector boson couplings is evident.

So far, we have only varied either $WW\gamma$ or $ZZ\gamma/Z\gamma\gamma$ couplings. If the three boson vertices contributing to $W\gamma$ and $Z\gamma$ production simultaneously deviate from the SM, cancellations may occur between the contributions to $\sigma(W^{\pm}\gamma)$ and $\sigma(Z\gamma)$. Couplings corresponding to operators of different dimension in the effective Lagrangian have a different high-energy behavior, and thus do not cancel at a substantial level in the cross-section ratios. On the other hand, the effects of $WW\gamma$ and $ZZ\gamma/Z\gamma\gamma$ couplings of equal dimension may cancel almost completely in $\mathcal{R}_{\gamma,l}$ and $\mathcal{R}_{\gamma,\nu}$, if the couplings are similar in magnitude. This is illustrated in Fig. 14, where we show $\mathcal{R}_{\gamma,\nu}^{-1}$ versus $p_T^{\min}(\gamma)$ for the SM (solid line), and two combinations of anomalous $WW\gamma$ and $ZZ\gamma$ couplings. The error bars in Fig. 14 display the statistical errors expected for $\int\mathcal{L}dt=25$ pb^{-1} and $W\to e\nu$ decays. The dashed line shows the expected result for $\lambda_0=1.7$ and $h_{30}^Z=1.5$. Both couplings correspond to operators of dimension six in the effective Lagrangian. It is clear that, for these couplings and with the integrated luminosity expected from the current Fermilab Tevatron run, the deviation from the SM cannot be seen. The dotted line in Fig. 14 shows $\mathcal{R}_{\gamma,\nu}^{-1}$ for $\Delta\kappa_0=2.6$ and $h_{40}^Z=0.075$. $\Delta\kappa_0$

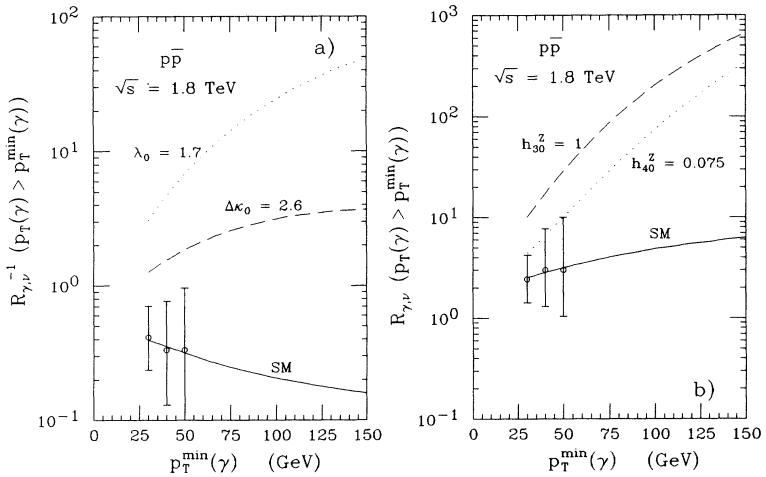

FIG. 13. (a) The inverse cross-section ratio $\mathcal{R}_{\gamma,\nu}^{-1}$ at the Tevatron versus $p_T^{\min}(\gamma)$. The curves are for the SM (solid), $\Delta\kappa_0=2.6$ (dashed), and $\lambda_0=1.7$ (dotted). A dipole form factor ($n=2$) with $\Lambda=750$ GeV is used to obtain the curves for nonstandard couplings. Only one $WW\gamma$ coupling is varied at a time. All $ZZ\gamma$ and $Z\gamma\gamma$ couplings are assumed to vanish identically. (b) The cross-section ratio $\mathcal{R}_{\gamma,\nu}$ at the Tevatron versus $p_T^{\min}(\gamma)$. The curves are for the SM (solid), $h_{30}^Z=1$ (dashed), and $h_{40}^Z=0.075$ (dotted). For the form factor parameters [see Eq. (3.9)] we assume $n=3$ ($n=4$) for h_{30}^Z (h_{40}^Z) with $\Lambda=750$ GeV. Only one $ZZ\gamma$ coupling is varied at a time. Anomalous $WW\gamma$ and $Z\gamma\gamma$ couplings are assumed to vanish identically. The cuts imposed are summarized in Eqs. (2.4) and (2.7). The error bars indicate the expected statistical errors for an integrated luminosity of 25 pb^{-1} for $W\to e\nu$ decays.

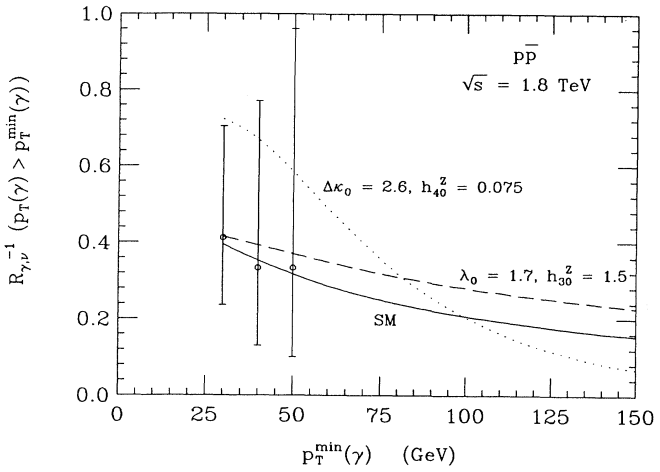

FIG. 14. The inverse cross-section ratio $\mathcal{R}_{\gamma,\nu}^{-1}$ at the Tevatron versus $p_T^{\min}(\gamma)$. The curves are for the SM (solid), $\Delta\kappa_0=2.6$, $h_{40}^Z=0.075$ (dashed), and $\lambda_0=1.7$, $h_{30}^Z=1.5$ (dotted). The cuts imposed are summarized in Eqs. (2.4) and (2.7). For anomalous $WW\gamma$ couplings a dipole form factor ($n=2$) is used. For nonstandard $ZZ\gamma$ couplings we assume $n=3$ ($n=4$) for h_{30}^Z (h_{40}^Z). The form factor scale is assumed to be $\Lambda=750$ GeV. The error bars indicate the expected statistical errors for an integrated luminosity of 25 pb^{-1} for $W\to e\nu$ decays.

corresponds to a dimension four operator, whereas h_{40}^Z originates from an operator of dimension eight in the effective Lagrangian. At small minimum photon transverse momenta, the effects of the anomalous $WW\gamma$ coupling dominate, and the inverse cross-section ratio is larger than expected in the SM. For larger values of $p_T^{\min}(\gamma)$, the influence of the higher-dimensional coupling on the $Z\gamma$ cross section increases, and $\mathcal{R}_{\gamma,\nu}^{-1}$ drops below the SM value. Only for $p_T^{\min}(\gamma)\approx 100$ GeV do the effects of the two nonstandard contributions cancel. Although no substantial cancellations over an extended region of $p_T^{\min}(\gamma)$ occur between $\Delta\kappa$ and h_4^Z, the error bars in Fig. 14 indicate that it will be difficult to discriminate between the SM prediction and the dotted curve at a statistically significant level with the data expected from the current Fermilab Tevatron run.

Possible cancellations between anomalous $WW\gamma$ and $ZZ\gamma/Z\gamma\gamma$ couplings in $\mathcal{R}_{\gamma,l}$ and $\mathcal{R}_{\gamma,\nu}$ can be excluded through a measurement of the ratios $\mathcal{R}_{W\gamma}$ and $\mathcal{R}_{Z\gamma}$. Since the three vector boson vertices do not enter the quantity in the denominator, and $\mathcal{R}_{W\gamma}$ ($\mathcal{R}_{Z\gamma}$) is only sensitive to $WW\gamma$ ($ZZ\gamma/Z\gamma\gamma$) couplings, cancellations between the effects of nonstandard $WW\gamma$ and $ZZ\gamma/Z\gamma\gamma$ couplings cannot occur in these cross-section ratios. The SM result for $\mathcal{R}_{W\gamma}$ ($\mathcal{R}_{Z\gamma}$) versus $p_T^{\min}(\gamma)$ is compared to $\sigma(W\gamma)/\sigma(W)$ [$\sigma(Z\gamma)/\sigma(Z)$] in the presence of anomalous $WW\gamma(ZZ\gamma)$ couplings in Fig. 15(a) [Fig. 15(b)]. The error bars indicate the statistical errors expected for 25 pb^{-1}, taking only the decays $W\to e\nu$ and $Z\to e^+e^-$ into account. Because of the large number of W bosons expected, the statistical error of $\mathcal{R}_{W\gamma}$ is considerably smaller than that of $\mathcal{R}_{\gamma,l}$ and $\mathcal{R}_{\gamma,\nu}$. In the current Fermilab Tevatron run it should be possible to measure $\mathcal{R}_{W\gamma}$ for minimum photon transverse momenta of up to $p_T^{\min}(\gamma)\approx 50$ GeV. The sensitivity of $\mathcal{R}_{V\gamma}$ ($V=W,Z$) to anomalous couplings is quite similar to that of $\mathcal{R}_{\gamma,\nu}$. Similar to the situation encountered for $\mathcal{R}_{\gamma,l}$, deviations from the SM predictions are less pronounced in $\mathcal{R}_{W\gamma}$ versus $m_{\min}$ than for the cross-section ratio as a function of $p_T^{\min}(\gamma)$.

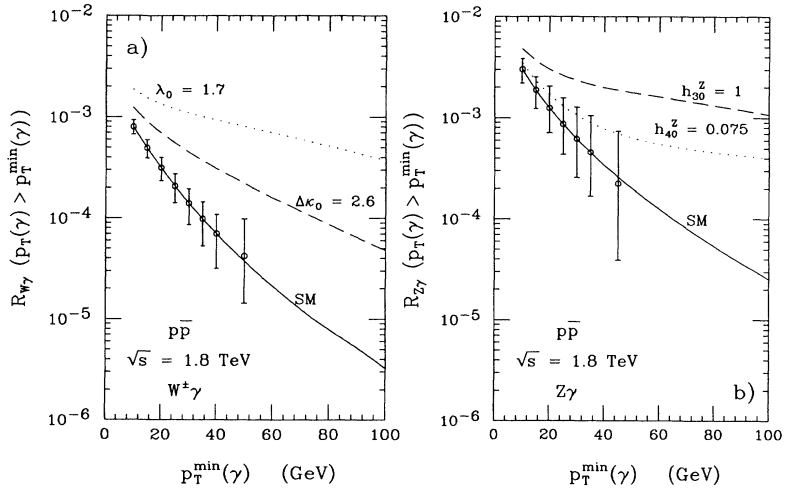

FIG. 15. (a) The cross-section ratio $\mathcal{R}_{W\gamma}$ at the Tevatron versus $p_T^{\min}(\gamma)$. The curves are for the SM (solid), $\Delta\kappa_0=2.6$ (dashed), and $\lambda_0=1.7$ (dotted). A dipole form factor ($n=2$) with $\Lambda=750$ GeV is used to obtain the curves for nonstandard couplings. Only one $WW\gamma$ coupling is varied at a time. (b) The cross-section ratio $\mathcal{R}_{Z\gamma}$ at the Tevatron versus $p_T^{\min}(\gamma)$. The curves are for the SM (solid), $h_{30}^Z=1$ (dashed), and $h_{40}^Z=0.075$ (dotted). For the form factor parameters we assume [see Eq. (3.9)] $n=3$ ($n=4$) for h_{30}^Z (h_{40}^Z) with $\Lambda=750$ GeV. Only one $ZZ\gamma$ coupling is varied at a time. Anomalous $Z\gamma\gamma$ couplings are assumed to vanish identically. The cuts imposed are summarized in Eqs. (2.4)–(2.7). The error bars indicate the expected statistical errors for an integrated luminosity of 25 pb^{-1} for $W\to e\nu$ and $Z\to e^+e^-$ decays.

C. Sensitivity limits

As we have demonstrated so far, the cross-section ratios listed in Eqs. (1.2)–(1.5) are sensitive indicators of anomalous couplings. We now want to make this statement more quantitative by deriving those values of $\Delta\kappa_0$, λ_0, and h_{i0}^V ($V=\gamma,Z$) which would give rise to a deviation from the SM at the level of one or two standard deviations in the various cross-section ratios. We assume an integrated luminosity of 25 pb^{-1} at the Fermilab Tevatron and the cuts listed in Eqs. (2.4)–(2.7). For $\mathcal{R}_{\gamma,\nu}$ the photon transverse momentum cut is increased to $p_T(\gamma)>30$ GeV, in order to reduce backgrounds from prompt photon and two-jet production. Sensitivity limits are calculated for form factors of the form given in Eq. (3.9) with $\Lambda=750$ GeV, $n=2$ for the $WW\gamma$ couplings $\Delta\kappa_0$ and λ_0, and $n=3$ ($n=4$) for $h_{10,30}^V$ ($h_{20,40}^V$) ($V=\gamma,Z$).

Our analysis is based on cross-section ratios obtained in the Born approximation and takes into account the expected theoretical and systematic uncertainties. Based on the results presented in Sec. II C, we roughly estimate the combined theoretical and systematic uncertainties from the parametrization of the parton distribution functions, the choice of the factorization scale Q^2, and higher-order QCD corrections to be about 10% for $\mathcal{R}_{\gamma,\nu}$ and $\mathcal{R}_{\gamma,l}$, 20% for $\mathcal{R}_{W\gamma}$, and approximately 15% for $\mathcal{R}_{Z\gamma}$ for the range of photon transverse momenta accessible in the current Fermilab Tevatron run. In order to obtain these numbers we have added the various contributions in quadrature. Possible systematic errors originating from background processes are ignored. In estimating the uncertainties from higher-order QCD corrections, we have assumed that the photon isolation cut (2.13) and the central jet veto of Eq. (2.14) are imposed in addition to cuts of Eqs. (2.4)–(2.7).

From the discussion in Sec. III B it is clear that, in most cases, the best sensitivity limits are obtained if the ratios are viewed as functions of the minimum photon transverse momentum. In the following we therefore derive bounds only for cross-section ratios viewed as a function of $p_T^{\min}(\gamma)$. In the ratios of $Z\gamma$ to $W^{\pm}\gamma$ cross sections we vary either $WW\gamma$ or $ZZ\gamma$ couplings. However, interference effects between $\Delta\kappa_0$ and λ_0, and between the various $ZZ\gamma$ couplings h_{i0}^Z, are fully taken into account in our analysis. Interference effects between $ZZ\gamma$ and $Z\gamma\gamma$ couplings are expected to be small [2] and are ignored. Sensitivity limits for h_{i0}^{γ} are nearly identical to those derived for h_{i0}^Z. Furthermore, bounds for the CP-violating couplings $h_{10,20}^Z$ virtually coincide with those for $h_{30,40}^Z$. We therefore concentrate on $\Delta\kappa_0$, λ_0, h_{30}^Z, and h_{40}^Z in the following.

To estimate the sensitivity bounds which can be achieved at the Fermilab Tevatron, we use the maximum likelihood technique. The likelihood function is calculated using binomial probability distributions for the cross-section ratios [41]. The minimum photon transverse momentum is increased in steps of at least 5 GeV, starting at $p_T^{\min}(\gamma)=10$ GeV for $\mathcal{R}_{V\gamma}$ and $\mathcal{R}_{\gamma,l}$, and at $p_T^{\min}(\gamma)=30$ GeV for $\mathcal{R}_{\gamma,\nu}$. For smaller steps in $p_T^{\min}(\gamma)$, the cross-section ratios for different minimum photon transverse momenta are strongly correlated, resulting in overly optimistic sensitivity limits.

The resulting bounds for $\Delta\kappa_0$, λ_0, and $h_{30,40}^Z$ are presented in Table I. Because of the larger statistical errors in $\mathcal{R}_{\gamma,l}$, the limits achievable from this ratio are about 20–30 % weaker than those from the other cross-section ratios. The 95% C.L. bounds from $\mathcal{R}_{\gamma,\nu}$ and $\mathcal{R}_{V\gamma}$ ($V=W,Z$) are quite similar. The larger statistical errors in $\mathcal{R}_{\gamma,\nu}$ are almost completely compensated by the smaller systematic and theoretical errors. Table I clearly demonstrates the advantage of $\mathcal{R}_{\gamma,\nu}$ due to the larger branching ratio of the $Z\to\bar{\nu}\nu$ decay. The limits on the $WW\gamma$ couplings $\Delta\kappa_0$ and λ_0 depend only slightly on the form factor scale, whereas the bounds on $h_{30,40}^Z$ can easily change by a factor 3–6 if Λ is varied by a factor 2 (Ref. [2]).

At Fermilab Tevatron energies, non-negligible interference effects are found between $\Delta\kappa$ and λ, and h_3^Z and h_4^Z. As a result, different anomalous contributions to the helicity amplitudes may cancel partially, resulting in weaker bounds than if only one coupling at a time is allowed to deviate from its SM value. These effects are fully taken into account in Table I. If only one coupling is varied at a time, the limits of Table I for $\Delta\kappa_0$ and λ_0 improve by 10–30 %. For example, one finds

$$\Delta\kappa_0=0^{+0.9}_{-0.7}\ \ (\text{for } \lambda_0=0)$$

and (3.11)

$$\lambda_0=0^{+0.28}_{-0.29}\ \ (\text{for } \kappa_0=1)\ ,$$

at the 1σ level from $\mathcal{R}_{\gamma,\nu}$. With $\int\mathcal{L}dt=25$ pb^{-1}, the present UA2 limit for κ (λ) [see Eq. (3.5)] thus may be

TABLE I. Sensitivities achievable at the 1σ and 2σ confidence levels (C.L.) for the anomalous $WW\gamma$ and $ZZ\gamma$ couplings $\Delta\kappa_0$, λ_0, h_{30}^Z, and h_{40}^Z from the cross-section ratios $\mathcal{R}_{\gamma,l}$, $\mathcal{R}_{\gamma,\nu}$, $\mathcal{R}_{W\gamma}$, and $\mathcal{R}_{Z\gamma}$, for an integrated luminosity of 25 pb^{-1} at the Fermilab Tevatron. The procedure used to extract the sensitivity bounds is described in the text. The limits for $\Delta\kappa_0$ (h_{30}^Z) apply for arbitrary values of λ_0 (h_{40}^Z) and vice versa. For the form factors we use Eq. (3.9) with $\Lambda=750$ GeV, $n=2$ for $WW\gamma$ couplings, and $n=3$ ($n=4$) for h_{30}^Z (h_{40}^Z), respectively. The W and Z decay channels into muons are not included in deriving the sensitivity limits. Anomalous $Z\gamma\gamma$ couplings are assumed to be zero.

Coupling	C.L.	$\mathcal{R}_{\gamma,l}$	$\mathcal{R}_{\gamma,\nu}$	$\mathcal{R}_{W\gamma}$
$\Delta\kappa_0$	2σ	$+2.5$	$+1.7$	$+1.7$
		-2.0	-1.3	-1.3
	1σ	$+1.8$	$+1.2$	$+1.5$
		-1.3	-0.9	-1.1
λ_0	2σ	$+0.84$	$+0.49$	$+0.52$
		-0.98	-0.57	-0.60
	1σ	$+0.54$	$+0.32$	$+0.44$
		-0.69	-0.40	-0.55
Coupling	C.L.	$\mathcal{R}_{\gamma,l}$	$\mathcal{R}_{\gamma,\nu}$	$\mathcal{R}_{Z\gamma}$
h_{30}^Z	2σ	±1.0	±0.8	±0.9
	1σ	±0.7	±0.5	±0.7
h_{40}^Z	2σ	±0.16	±0.13	±0.14
	1σ	±0.11	±0.09	±0.11

improved by up to a factor 3 (5). For the form factor parameters used, the bounds for h_{30}^Z and h_{40}^Z in Table I improve by a factor 1.6–2 if only one coupling is varied at a time.

The sensitivity to anomalous couplings stems from regions of phase space where the anomalous contributions to the cross sections are considerably larger than the SM expectation. As a result, the bounds scale essentially like $(\int \mathcal{L} dt)^{1/4}$. Therefore, increasing the integrated luminosity at the Fermilab Tevatron to 100 pb^{-1}, as foreseen by the end of 1994, will improve the sensitivity limits of Table I by about a factor 1.4. Because of smaller experimental, theoretical, and systematic uncertainties of the cross-section ratios, the resulting bounds may be considerably better than those expected from analyzing the $p_T(\gamma)$ distribution [1,2].

The bounds listed in Table I have been obtained for a generic set of cuts [Eqs. (2.4)–(2.7)]. They also depend somewhat on the exact procedure used to extract the limits. For example, increasing $p_T^{\min}(\gamma)$ in steps of 30 GeV, weakens the bounds by 20–30%. Our limits thus should be regarded as guidelines, illustrating the capabilities of CDF and D0 in improving our knowledge of $WW\gamma$ and $ZZ\gamma/Z\gamma\gamma$ couplings within the immediate future.

As we have mentioned before, for 25 pb^{-1} the sensitivity of the cross-section ratios to anomalous couplings is limited mostly by statistical errors. For this situation, a calculation of the ratios at tree level is completely sufficient. For larger integrated luminosities, the theoretical and systematic errors become more important in limiting the sensitivity bounds which can be achieved. These errors could be improved substantially if a full $O(\alpha_s)$ calculation of the ratios for general $WW\gamma$ and $ZZ\gamma/Z\gamma\gamma$ couplings is carried out. This would, in particular, reduce the uncertainty originating from the choice of the factorization scale Q^2, which dominates the systematic and theoretical errors in $\mathcal{R}_{W\gamma}$ and $\mathcal{R}_{Z\gamma}$ at large $p_T^{\min}(\gamma)$.

IV. SUMMARY AND CONCLUSIONS

In this paper we have studied the theoretical aspects of cross-section ratios for the processes $p\bar{p}\to W^{\pm}\gamma$ and $p\bar{p}\to Z\gamma$ at Fermilab Tevatron energies. Four different ratios can be formed, which are listed in Eqs. (1.2)–(1.5). Compared to direct measurements of cross sections, experimental, theoretical, and systematic errors are expected to be significantly reduced in ratios of cross sections.

Our main results can be summarized as follows.

(1) The ratios

$$\mathcal{R}_{\gamma,l}=B(Z\to l^+l^-)\sigma(Z\gamma)/B(W\to l\nu)\sigma(W^{\pm}\gamma)$$

and

$$\mathcal{R}_{\gamma,\nu}=B(Z\to \bar{\nu}\nu)\sigma(Z\gamma)/B(W\to l\nu)\sigma(W^{\pm}\gamma)$$

as a function of the minimum photon transverse momentum, $p_T^{\min}(\gamma)$, increase sharply with $p_T^{\min}(\gamma)$ in the SM, reflecting the radiation zero which is present in the lowest order $q\bar{q}'\to W^{\pm}\gamma$ helicity amplitudes.

(2) The systematic and theoretical errors of $\mathcal{R}_{\gamma,l}$ and $\mathcal{R}_{\gamma,\nu}$ are significantly smaller than those of $\mathcal{R}_{V\gamma}=\sigma(V\gamma)/\sigma(V)$ $(V=W^{\pm},Z)$. Theoretical and systematic uncertainties are well under control for all cross-section ratios.

(3) Higher-order QCD corrections only partially cancel in the cross-section ratios, in particular, at large photon transverse momenta. The imperfect cancellations can be traced to a phase-space region where a high p_T photon is balanced by a quark jet which emits a W or Z boson almost collinear with the quark. By applying a modest central jet veto requirement [see Eq. (2.14)], the residual QCD corrections cancel almost completely in the cross-section ratios over a wide range of photon transverse momenta.

(4) The $W^{\pm}\gamma$ and $Z\gamma$ cross-section ratios listed in Eqs. (1.2)–(1.5) constitute powerful new tools which can be used to set new limits on physics beyond the SM. We have studied in detail the impact of nonstandard $WW\gamma$ and $ZZ\gamma/Z\gamma\gamma$ couplings on the cross-section ratios and have derived sensitivity limits (see Table I) based on an integrated luminosity of 25 pb^{-1} expected from the current Fermilab Tevatron run. For anomalous $WW\gamma$ couplings, these limits improve present hadron collider bounds up to a factor 3–5. The various cross-section ratios yield complementary information on the three vector boson couplings.

The bounds listed in Table I should be compared with theoretical expectations, existing low-energy limits, and constraints obtained from LEP I data. In models based on chiral perturbation theory, for example, one typically expects deviations from the SM of $\sim 10^{-2}$ (Ref. [42]). Although bounds can be extracted from low-energy and high-precision measurements at the Z pole, there are ambiguities and model dependencies in the results [43–45]. From loop contributions to $(g-2)_\mu$ one estimates [46] limits which are typically of order $1-10$. No rigorous bounds on $WW\gamma$ couplings can be obtained from LEP I data, if correlations between different contributions to the anomalous couplings are fully taken into account. Without serious cancellations among various one-loop contributions, one finds [45]

$$|\Delta\kappa|,|\lambda|\lesssim 0.5-1.5 \tag{4.1}$$

at the 90% C.L. from present data on S, T, and U (Ref. [47]) (or, equivalently, ϵ_1, ϵ_2, and ϵ_3 (Ref. [48])). The limits which can be obtained from data expected in the current Fermilab Tevatron run are already competitive with the bounds of Eq. (4.1). Constraints on $ZZ\gamma$ and $Z\gamma\gamma$ couplings from S, T, and U have not been calculated so far. LEP I data on radiative Z decays provide only very little information on the structure of the $ZZ\gamma/Z\gamma\gamma$ vertex [2].

Significant improvements of the bounds derived in Table I can be expected if an integrated luminosity of 100 pb^{-1} is accumulated at the Fermilab Tevatron, as fore-

seen by the end of 1994, and from W pair and $Z\gamma$ production at LEP II [37,49]. Finally, the LHC and SSC [6], and a linear e^+e^- collider with $\sqrt{s}=500$ GeV (Refs. [50,51]) will enable a measurement of the $WW\gamma$ and $ZZ\gamma/Z\gamma\gamma$ couplings at the 1% level. In view of our present poor knowledge of the self-interactions of W bosons, Z bosons, and photons, the limits which can be obtained from a measurement of the $W^{\pm}\gamma$ and $Z\gamma$ cross-section ratios with the data accumulated in the current Tevatron run will represent a major step forward towards a high-precision measurement of the three vector boson vertices.

ACKNOWLEDGMENTS

We would like to thank F. Halzen, S. Keller, G. Landsberg, and D. Zeppenfeld for stimulating discussions, and encouragement. We are also grateful to H. Baer for providing us with the FORTRAN code of Ref. [25]. One of us (U.B.) would like to thank the Fermilab Theory Group, where this work was completed, for its warm hospitality. This research was supported in part by the UK Science and Engineering Research Council, and in part by the U.S. Department of Energy under Grant No. DE-FG02-91ER40677 and Contract No. DE-FG05-87ER40319.

[1] U. Baur and E. L. Berger, Phys. Rev. D **41**, 1476 (1990).
[2] U. Baur and E. L. Berger, Phys. Rev. D **47**, 4889 (1993).
[3] F. Halzen and K. Mursula, Phys. Rev. Lett. **51**, 857 (1983); K. Hikasa, Phys. Rev. D **29**, 1939 (1984); N. G. Deshpande *et al.*, Phys. Rev. Lett. **54**, 1757 (1985); A. D. Martin, R. G. Roberts, and W. J. Stirling, Phys. Lett. B **189**, 220 (1987); E. L. Berger, F. Halzen, C. S. Kim, and S. Willenbrock, Phys. Rev. D **40**, 83 (1989).
[4] UA1 Collaboration, C. Albajar *et al.*, Phys. Lett. B **253**, 503 (1991); UA2 Collaboration, J. Alitti *et al.*, *ibid.* **276**, 365 (1992); CDF Collaboration, F. Abe *et al.*, Phys. Rev. D **44**, 29 (1991); Phys. Rev. Lett. **69**, 28 (1992).
[5] V. Barger, T. Han, J. Ohnemus, and D. Zeppenfeld, Phys. Rev. Lett. **62**, 1971 (1989); Phys. Rev. D **40**, 2888 (1989); **41**, 1715(E) (1990).
[6] U. Baur and D. Zeppenfeld, Nucl. Phys. **B308**, 127 (1988).
[7] J. Smith, D. Thomas, and W. van Neerven, Z. Phys. C **44**, 267 (1989).
[8] J. Ohnemus, Phys. Rev. D **47**, 940 (1993).
[9] R. Brown, D. Sahdev, and K. Mikaelian, Phys. Rev. D **20**, 1164 (1979); K. Mikaelian, M. Samuel, and D. Sahdev, Phys. Rev. Lett. **43**, 746 (1979); Zhu Dongpei, Phys. Rev. D **22**, 2266 (1980); C. J. Goebel, F. Halzen, and J. P. Leveille, *ibid.* **23**, 2682 (1981); S. J. Brodsky and R. W. Brown, Phys. Rev. Lett. **49**, 966 (1982); R. W. Brown, K. L. Kowalski, and S. J. Brodsky, Phys. Rev. D **28**, 624 (1983); M. A. Samuel, *ibid.* **27**, 2724 (1983).
[10] F. A. Berends *et al.*, Phys. Lett. **103B**, 124 (1981); P. Aurenche *et al.*, *ibid.* **140B**, 87 (1984); Nucl. Phys. **B286**, 553 (1987); V. Barger, T. Han, J. Ohnemus, and D. Zeppenfeld, Phys. Lett. B **232**, 371 (1989).
[11] CDF Collaboration, F. Abe *et al.*, Phys. Rev. D **45**, 3921 (1992).
[12] H. Wahl (private communication).
[13] J. Womersley (private communication); R. J. Madaras, in *The Fermilab Meeting,* Proceedings of the Annual Meeting of the Division of Particles and Fields of the APS, Batavia, Illinois, 1992, edited by C. Albright *et al.* (World Scientific, Singapore, 1993), Vol. I, p. 19; M. Cobal, in Proceedings of the Fourth Topical Seminar on the Standard Model and Just Beyond, San Miniato, Italy, 1992 (unpublished).
[14] S. Bethke and S. Catani, in *QCD and High Energy Hadronic Interactions,* Proceedings of the XXVIIth Rencontre de Moriond, Les Arcs, France, 1992, edited by J. Tran Thanh Van (Editions Frontieres, Gif-sur-Yvette, 1992), p. 203.
[15] P. N. Harriman, A. D. Martin, R. G. Roberts, and W. J. Stirling, Phys. Rev. D **42**, 798 (1990).
[16] J. Cortes, K. Hagiwara, and F. Herzog, Nucl. Phys. **B278**, 26 (1986); J. Stroughair and C. Bilchak, Z. Phys. C **26**, 415 (1984); J. Gunion, Z. Kunszt, and M. Soldate, Phys. Lett. **163B**, 389 (1985); J. Gunion and M. Soldate, Phys. Rev. D **34**, 826 (1986); W. J. Stirling *et al.*, Phys. Lett. **163B**, 261 (1985).
[17] CDF Collaboration, F. Abe *et al.*, Phys. Rev. Lett. **66**, 2951 (1991).
[18] A. D. Martin, W. J. Stirling, and R. G. Roberts, Phys. Rev. D **47**, 867 (1993).
[19] M. Glück, E. Reya, and A. Vogt, Z. Phys. C **53**, 127 (1992).
[20] J. Morfin and W. K. Tung, Z. Phys. C **52**, 13 (1991).
[21] J. F. Owens, Phys. Lett. B **266**, 126 (1991).
[22] NMC Collaboration, P. Amaudruz *et al.*, Phys. Lett. B **295**, 159 (1992).
[23] CCFR Collaboration, S. R. Mishra *et al.*, Institution Report No. NEVIS-1459 (unpublished).
[24] W. L. van Neerven and E. B. Zijlstra, Nucl. Phys. **B382**, 11 (1992).
[25] H. Baer and M. H. Reno, Phys. Rev. D **43**, 2892 (1991); **45**, 1503 (1992).
[26] S. Frixione, P. Nason, and G. Ridolfi, Nucl. Phys. **B383**, 3 (1992).
[27] CDF Collaboration, F. Abe *et al.*, Phys. Rev. Lett. **64**, 152 (1990).
[28] CDF Collaboration, F. Abe *et al.*, Phys. Rev. Lett. **65**, 224 (1990); Phys. Rev. D **43**, 2070 (1991).
[29] The LHC Study Group, Design Study of the Large Hadron Collider, CERN 91-03, 1991.
[30] U. Baur, T. Han, and J. Ohnemus, Phys. Rev. D (to be published).
[31] SDC Collaboration, E. L. Berger *et al.*, SDC Technical Design Report No. SDC-92-201, 1992 (unpublished).
[32] R. Barbieri, H. Harari, and M. Leurer, Phys. Rev. Lett. **141B**, 455 (1985).
[33] U. Baur and D. Zeppenfeld, Phys. Lett. B **201**, 383 (1988).
[34] W. J. Marciano and A. Queijeiro, Phys. Rev. D **33**, 3449 (1986); F. Boudjema, K. Hagiwara, C. Hamzaoui, and K. Numata, *ibid.* **43**, 2223 (1991).
[35] UA2 Collaboration, J. Alitti *et al.*, Phys. Lett. B **277**, 194 (1992).
[36] D. Benjamin, in Electroweak Interactions and Unified Field Theories, Proceedings of the XXVIIIth Rencontre de Moriond, Les Arcs, France, 1993 (unpublished).
[37] K. Hagiwara *et al.*, Nucl. Phys. **B282**, 253 (1987).
[38] C. N. Yang, Phys. Rev. **77**, 242 (1950).

[39] J. M. Cornwall, D. N. Levin, and G. Tiktopoulos, Phys. Rev. Lett. **30**, 1268 (1973); Phys. Rev. D **10**, 1145 (1974); C. H. Llewellyn Smith, Phys. Lett. **46B**, 233 (1973); S. D. Joglekar, Ann. Phys. (N.Y.) **83**, 427 (1974).

[40] CDF Collaboration, F. Abe *et al.*, Phys. Rev. Lett. **69**, 28 (1992).

[41] F. James and M. Roos, Nucl. Phys. **B172**, 475 (1980).

[42] J. Bagger, S. Dawson, and G. Valencia, Nucl. Phys. **B399**, 364 (1993).

[43] A. De Rújula *et al.*, Nucl. Phys. **B384**, 31 (1992); P. Hernández and F. J. Vegas, Phys. Lett. B **307**, 116 (1993).

[44] C. Burgess and D. London, Phys. Rev. Lett. **69**, 3428 (1992); McGill Report No. McGill-92/04, 1992 (unpublished); this issue, Phys. Rev. D **48**, 4326 (1993).

[45] K. Hagiwara, S. Ishihara, R. Szalapski, and D. Zeppenfeld, Phys. Lett. B **283**, 353 (1992); Phys. Rev. D **48**, 2182 1993.

[46] P. Méry, S. E. Moubarik, M. Perrottet, and F. M. Renard, Z. Phys. C **46**, 229 (1990).

[47] M. E. Peskin and T. Takeuchi, Phys. Rev. Lett. **65**, 964 (1990); Phys. Rev. D **46**, 381 (1992).

[48] G. Altarelli and R. Barbieri, Phys. Lett. B **253**, 161 (1991); G. Altarelli, R. Barbieri, and S. Jadach, Nucl. Phys. **B369**, 3 (1992).

[49] P. Méry, M. Perrottet, and F. M. Renard, Z. Phys. C **38**, 579 (1988).

[50] G. Gounaris *et al.*, in e^+e^- *Collisions at 500 GeV: The Physics Potential,* Proceedings of the Workshop, edited by P. Zerwas (DESY Report No. 92-123, Hamburg, Germany, 1992), Vol. B, p. 735; F. Boudjema, *ibid.*, p. 757.

[51] E. Yehudai, Phys. Rev. D **41**, 33 (1990); **44**, 3434 (1991); S. Y. Choi and F. Schrempp, Phys. Lett. B **272**, 149 (1991); O. Philipsen, Z. Phys. C **54**, 643 (1992); S. Godfrey and K. A. Peterson, Report No. OCIP/C 92-7, 1992 (unpublished).